LEVEL

AF INSTITUTE OF TECHNOLOGY

UNITED STATES AIR FORCE

AIR UNIVERSITY

AIR FORCE INSTITUTE OF TECHNOLOGY

Wright-Patterson Air Force Base, Ohio

78 06 15 071

AD A057362
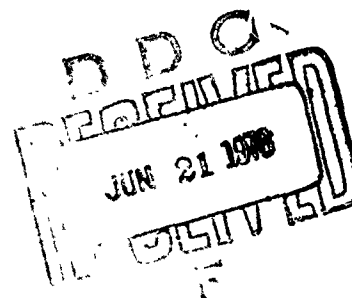
JUN 21 1978

AD No.
DDC FILE COPY

DIFFERENTIAL-HALL IMPURITY

PROFILING OF GaAs, CO-IMPLANTED

WITH Ga^+, C^+ AND As^+, C^+

THESIS

GEO/PH/77-4   Michael Stefiniw
                2Lt   USAF

78 06 15 071

DIFFERENTIAL-HALL IMPURITY PROFILING OF GaAs, CO-IMPLANTED WITH Ga$^+$, C$^+$ AND As$^+$, C$^+$ . .

Master's THESIS,

Presented to the Faculty of the School of Engineering

of the Air Force Institute of Technology

Air University

in Partial Fulfilment of the

Requirements for the Degree of

Master of Science

by

:

Michael Stefiniw B.E.

2Lt   USAF

Graduate Electro-Optics

Octo█████77   65 p.

012 225

Preface

From the start, this thesis has been most interesting and informative. It was most rewarding to do this thesis for two reasons. First, not much research has been done in dual implantations, and secondly, the results obtained suggest the possibilities which this field of work offers. Future work should be carried out on the carbon-ion for it shows the possibility of a useful dopant for submicron devices, since the diffusion is negligible up to annealing temperatures of 900°C.

I wish to thank the people who made this project possible for me. I would particularly like to thank Jim Ehret who implanted my samples, Charles Geesner for capping my samples as quickly as possible and Captain David Lank for letting me use his computer profiling program and Bok Kyoon Shin who was my lab advisor and gave me many suggestions. Additional thanks go to my project sponsor Yoon Soo Park and faculty advisor Dr. T. Luke.

Table of Contents

List of Figures

v

List of Tables

Abstract

Co-implantation of Ga^+ or As^+ with C^+ has produced p-type conduction in GaAs substrate. Sheet resistivity and Hall effect measurements were made and differential Hall effect measurements were carried out using a guarded van der Pauw system. These measurements were carried out on 10^{12}, 10^{13}, and 10^{14} dosage samples annealed at 600, 700, 800 and 900°C for fifteen minutes. Doping efficiency of 87% was obtained in the 800°C annealed sample implanted with 10^{13} ins/cm^2 of Ga^+ and C^+, which is much higher than for the C^+ alone implants. Samples annealed at 900°C, 10^{14} ins/cm^2 of Ga^+ and C^+ had an efficiency of 32.3%, which is also higher than the C^+ alone implants. Carbon implants alone had a 57% efficiency when annealed at 900°C with a dose of 10^{13}/cm^2 and 9.5% when annealed at 900°C with a dose of 10^{14}/cm^2, which verifies previous work done with carbon implants.

I. Introduction

The need for devices such as laser diodes, microwave components, integrated optics, and digital IC's with multigigabit data rates has prompted research in the ion implantation field of semiconductor fabrication. The reason for using ion implantation and why so much time and effort is being placed on it, is that the doping densities, distribution and layer thickness are thought to be controlled more precisely than with diffusion or epitaxial growth.

Ion implantation is a relatively new method of doping GaAs semiconductors but has been successfully used in devices with silicon substrates. It is a process by which impurity ions are accelerated by a particle accelerator and implanted into the substrate. The depth to which the impurity ions will penetrate is dependent upon the ion mass, energy of the beam and crystal orientation. After the implantation crystal lattice damage exists which must be annealed by heat treatment. This process is also used to electrically activate the impurity ions for conduction by moving them into the crystal sites. However, the annealing temperature required to effectively do the job exceeds the temperature where the GaAs surface begins to decompose. To prevent or reduce this effect the sample is encapsulated by a dielectric layer of Si_3N_4, approximately 1000 Å thick. This layer is placed on the sample after implantation and before annealing. The dielectric layer is etched away when electrical measurements are performed on the sample. The guarded van der Pauw measuring system is used to acquire the crystal and Hall voltages of the samples. Electrical profiles are obtained on the 900°C annealed samples by a successive etching technique.

ANGSTROM

1

Statement of Problem

There has been very little research done in the area of carbon ion implanted gallium arsenide. The research that has been performed has produced results demonstrating that p-type layers can be produced in ion implanted samples. There has been no research investigating the possibility of forming an n-type layer in GaAs with carbon.

The problem to be examined in this thesis is that of forming an n-type layer in GaAs, by co-implantation of carbon ions with arsenic incoporation. The possibility of increasing the electrical activity of the carbon ions in p-type material by co-implantation with gallium is also examined. The former objective is worth the time to investigate because experimentation has shown that the group IV impurity atom tend to replace the larger of the two-sub-lattice atoms which form the compound (Ref 2:70). This would have technological value in that submicron devices of both n- or p-type layers could be formed by doping with carbon ions and controlling the GaAs stoicheometry by either Ga or As co-implantation.

Summary of Current Knowledge

No work has specifically been done in obtaining an n-type layer in GaAs using carbon ion implantation. However, all group IV elements have been successfully used in forming n-type layers, with the exception of carbon. Previously, some work was done in p-type layer implants using carbon but the doping efficiencies were so low that it was believed carbon might be useless as an impurity for ion implantation. Some research done recently along these lines has been concerned with obtaining p-type layer in GaAs using carbon ion implantation (Ref 4). The

results were a great improvement over previous work, in some cases, doping efficiencies ($n \equiv P_s/\phi$) of 50% were obtained, compared with previous efficiencies of 7%. Co-implantation has been shown to enhance donor and acceptor activity in selenium and silicon implants (Ref 5,6). The problems encountered are complex but the potential of this technique warrants work in this area.

Theory

The theory behind the work performed here was developed by Heckingbottom and Ambridge for binary compound semiconductors such as gallium arsenide (Ref 1). The reason such a theory was developed stemmed from the great difference in implanting into a element such as silicon and binary compounds. The model to represent the doping of silicon is as follows, using Kroger-Vink notation (see Appendix A):

$$F(g) \rightleftharpoons F_{Si}{}^{X} \tag{1}$$

$$F_{Si}{}^{X} \rightleftharpoons F_{Si}' + h^{\bullet} \tag{2}$$
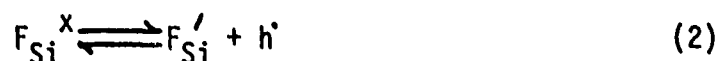
The situation is much simpler here due to the fact that there is only one sub-lattice to build up. When an dopant is implanted in the binary compound case, only one sub-lattice is built and a compensating defect is formed (Ref 1). The situation can be described as follows:

$$F(g) \rightleftharpoons F_{As}{}^{X} + V_{GA}{}^{X} \tag{3}$$

$$V_{GA}{}^{X} \rightleftharpoons V_{GA}' + h^{\bullet} \tag{4}$$
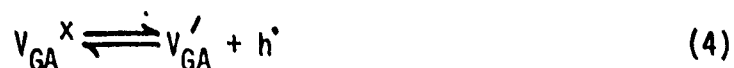
which disrupts GaAs stoicheometry. The method of controlling this non-stoicheometry is to implant an equal amount of the host atom on the other sublattice when the dopant is being implanted.

This is only part of the sublattice control which must be done. Time dependent non-stoicheometry arises during the annealing process. The encapsulation process is used to combat this out-diffusion.

Scope

The work performed is limited to electrical measurements and profiling using the van der Pauw system. Due to the time involved, surface measurements were taken for all the samples while only five profiles were completed. This gave some insight to the processes taking place but is in no way complete. Glow Discharge Optical Spectroscopy which would give a spatial distribution of the total impurity, was not done, due to the lack of equipment accessibility. Two such profiles, one obtained electrically and the other obtained optically, could be compared and correlated. This would give us a better understanding of the distribution of impurity ions that are used in this study.

In the following chapter, the various sections discuss sample preparation, implantation, annealing, encapsulation, differential Hall technique, and data processing. The results are presented in graphical form so that the trends of the implants can be visualized. Following this chapter, a discussion is presented on what is believed to be happening, and why. A summary, conclusion and recommendation section makes up the final portion of this study.

4

II. Experimental Procedure

This chapter on experimental procedure will be made up of several subsections. The sections will be covered in the following order: sample preparation, implantation procedure, encapsulation and annealing process, data acquisition and processing and finally equipment list and figure of set-up.

The gallium arsenide used in this experiment was obtained from Laser Diodes Laboratories and ordered chromium doped to make it semi-insulating. Three wafers were used approximately 2 1/2 inches in diameter and 20 mils thick. They were all from the same boule, two wafers being next to each other, while the third was from a different part of the same boule. The samples have a resistivity of 10^9 ohms and a chromium concentration of $\sim 10^{17}/cm^3$ as measured by mass-spectroscopic analysis technique.

Sample Preparation

The wafers were cut into twenty-five samples, 5mm square making maximum use of the wafer. A wafer scriber was used to cut the wafers, holding them in place by a vacuum chuck. This size was found to be the best to handle and made implanting much easier. The reason for this is that four samples could be implanted at the same time with the same dose.

The samples were then cleaned to remove any organic substance or film which might have been present on the polished surface. The sample was placed in a solution of aquasol concentrate and water in a ratio of 10:1 by volume. This soap solution, in a beaker was placed in an ultra-sonic cleaner containing water filled to the same height as the soap

solution in the beaker. The sample was then allowed to clean for five minutes. After cleaning in the soap solution, the sample was rinsed with deionized water for one minute to completely remove the soap. Then the sample was rinsed with the following solvents: trichlorethylene ($CL_2C:CHCL$) for twenty seconds, acetone (CH_3COCH_3) for twenty seconds and finally methanol (CH_3OH) for twenty seconds, in that order. The sample was then blown dry by a spray of purified nitrogen gas. The surface was then checked for any organic residue and surface oxidation by dark field microscopy. If either of these were found not to be removed by the above procedure, the cleaning process was repeated until all the residue and oxidation was gone. When the surface is clean of residue, the free etch (described next) was used to clean and remove any mechanical damage which might be present. (This is necessary for coherent adhesion of the capping material.) The free etch is composed of the following chemical mixtures: $H_2O:30\% H_2O_2:H_2SO_4$ in a volume ratio of 1:1:5. The chip was placed in the etch for one minute while being constantly agitated. This is done so that pits or surface deterioration will not occur. When removed from the etch the sample was immediately rinsed with deionized water for one minute to remove any acid from the surface and blown dry with an inert gas. After the above procedure is accomplished the chip was placed in the ion implantation facility to protect it from the formation of oxides or organic residue on the surface.

Implantation Procedure

The 150Kev ion accelerator used in the following work was an Accelerator Inc., Modified Implanter-I, which has been highly modified

6

for the work being done at the Air Force Avionics Laboratory (AFAL). The machine has two means of generating ions for implantation: either a hot-cathode source or a radio frequency discharge. The hot-cathode source is used to ionize solid materials, while the radio frequency (RF) discharge is used for ionizing gases. In the present investigation, both sources were used to obtain the ions for implantation. The samples which were implanted with carbon ions (C^+) only used the RF discharge to obtain C^+ from carbon dioxide (CO_2) gas. The samples which had dual implants had to use both sources. The first batch of dual implant samples were implanted with arsenic, obtained from arsenic metal, and with carbon, in equal dosage. The second batch of dual implants were implanted first with gallium obtained from gallium triflouride and with carbon, also in equal dosage. Three doping concentrations ($10^{12}/cm^2$, $10^{13}/cm^2$ and $10^{14}/cm^2$) were used for each of the three types of materials (GaAs: C^+, GaAs: As^+, C^+ and GaAs: Ga^+, C^+) making nine different types of samples in all. The energy of the implants were 60Kev for the C^+ and 120Kev for the gallium and arsenic ions. These were not the energies which were desired to implant the ions but they were only what the accelerator could handle. It would have been preferred to implant the carbon ion at 120Kev and gallium and arsenic ions at 700Kev, so that the two distributions of implants would overlap more completely and minimize surface erosion during implantation. The energies used did show some overlapping of distributions, but not as much as was desired.

Encapsulation and Annealing Conditions

After the implantation of the ions, the samples were encapsulated

with silicon nitride (Si_3N_4) a material which has been well documented
in the literature to be superior to silicon dioxide (SiO_2) for GaAs
encapsulation((Ref 4). The cap was used in this thesis to prevent
gallium from out-diffusing, which occurs at temperatures of 600°C
(Ref 4).

All the samples were coated with approximately 1000Å of Si_3N_4, as
determined by the color change which takes place on the surface of the
sample during the encapsulation process (Appendix C). This cap can
also be placed on the surface prior to implantation so as to control
the position and shape of the distribution.

The pyrolytic reactor used in this thesis for encapsulation was
designed based on a MIT Lincoln Laboratories set-up (Ref 3:26). It is
possible to encapsulate samples with two different types of films using
this system, SiO_2 or Si_3N_4. For this experiment, Si_3N_4 film was de-
posited on the sample by using specific amounts of nitrogen (N_2),
ammonia (NH_3) and silane (SiH_4) mixed in a glass bell chamber. The
chamber was first evacuated to remove impurities from the system, after
which it was purged with nitrogen. The sample rested on a carbon strip
whose temperature was controlled, thus allowing the reaction which is
necessary for the deposition of the film. As the chamber was being
purged with nitrogen, the sample was brought to 200°C, helping to pre-
vent any silicon dioxide from forming on the surface. Formation of
silicon dioxide would prevent coherent adhesion of the Si N film. After
purging for a few minutes, controlled amounts of 5% saline and liquid
ammonia were introduced which had been previously diluted with equal
amounts of nitrogen. These mixtures were added to the chamber from

8

above where they were allowed to mix for a few seconds. The temperature was then brought up quickly to 740°C for thirty seconds (for 1000Å thick film), during which time the gas mixtures reacted to form a film on the sample which could be observed by the change in color of the semiconductor surface. After thirty seconds the temperature was brought down immediately to 200°C, during which time the chamber was purged of the gas mixture using nitrogen. The film was then checked for its true thickness using a Gaetner Scientific ellipsometer. This verified the thickness used on the samples in this thesis of approximately 1000Å-1200Å. The flow rates of saline, ammonia and nitrogen, the carbon strip temperature during deposition, and the time allowed for deposition are documented in Appendix B.

After the Si_3N_4 was deposited, the samples were annealed at 600°C, 700°C, 800°C and 900°C (15 minutes at each temperature) in a flowing hydrogen ambient. Three samples of the same implants but of different doses were all annealed at once to save time. When the samples were annealed, a tub of gallium was placed with them so as to help combat the out-diffusion of gallium (Fig. 1). To minimize thermal shock, the
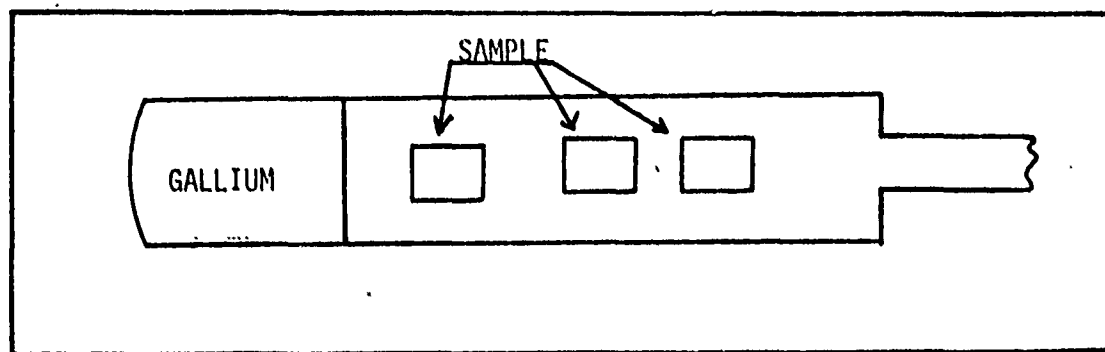
Fig. 1. Set-up for annealing samples

9

samples to be annealed were placed in the holder outside the quartz tube furnace, as it was brought up to temperature. The hydrogen gas was first run through a hydrogen purifier before flowing into the furnace. The hydrogen flows through the furnace at 226.6 cubic centimeters per minute during the warm up period, annealing process and cool down. After annealing, the samples were pulled from the heating area but not removed from the furnace, thereby allowing them to cool down to room temperature. During cool down, hydrogen still flows through the furnace and over the samples, at the same time being bled off by burning on a platinum wire. After cooling down, the samples were removed from the furnace and were ready to be profiled once the cap was removed and contacts were attached to the samples.

The cap was removed using a 48% reagent hydrofluoric acid (HF), for usually ten minutes or as long as required. Then the sample was washed by flowing deionized water over it for one minute (to remove the acid from the surface) and blown dry using nitrogen gas.

Contacts were then ultrasonically soldered to the four corners of the sample using pure indium. After soldering, the contacts were checked with a curve tracer to make sure t!ey were ohmic (Fig. 2). If they were not ohmic, the contacts would be resoldered in an attempt to correct the problem. If, after resoldering the contacts were still rectifying they could be sintered by heating the sample to 450°C. This would reduce the strain in the crystal and the contacts would be more ohmic in nature as a result of the alloying process.
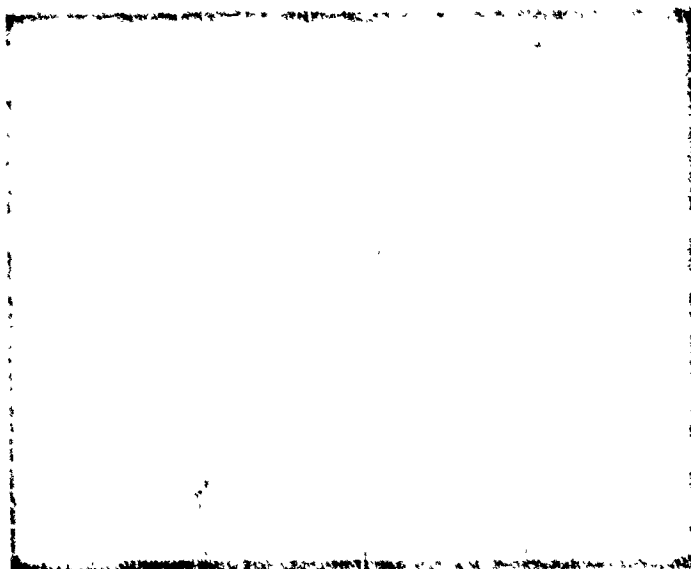
Fig. 2. I-V curve for sample contact

Data Acquisition and Processing

The system used for data acquisition was a van der Pauw measurement system composed of guarded unity-gain amplifiers (Fig. 3) which provide an input impedance of 10^{14} ohms. This system was used at the Aerospace Research Laboratory and designed by B. K. Shin. It has a variety of measurement capabilities such as a guarded Hall and van der Pauw configurations and continuous temperature changes to $4^{\circ}K$ using the Air Product Helitran.

The van der Pauw method was the only one used in this thesis to acquire the data. There are advantages in using this method in that the samples were small and only four contacts were required on the periphery of an arbitrarily shaped sample. When using the van der Pauw method, it is required to measure voltage across two leads while current

11
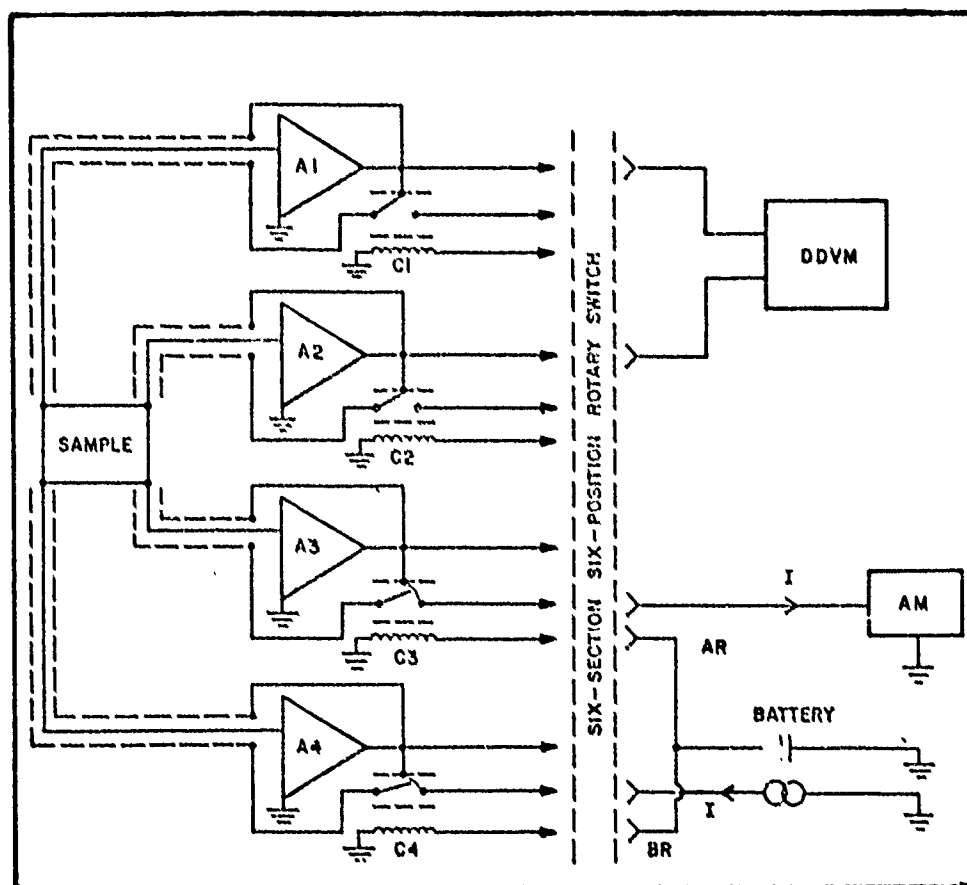
Fig. 3. System diagram of guarded van der Pauw
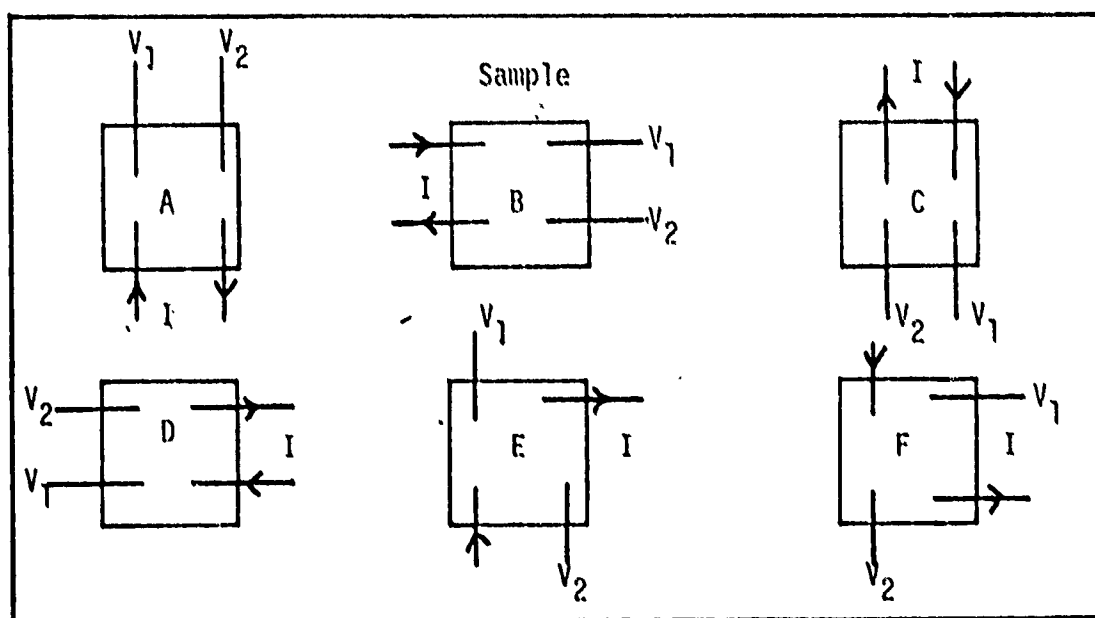
Fig. 4. Sample configurations

is passed through the opposite leads as shown in Fig. 4 (a-d). Voltage readings were made by interchanging the leads to the sample. This was done by a six-position rotary switch which is marked the same as the configurations in Fig. 4. The last two configurations (e & f) were used to take Hall voltage readings when a magnetic field is applied prependicula- to the sample. A total of eight voltage measurements were made on configurations a-d by reversing the current direction on each configuration. This way, after averaging all the crystal voltages, a more realistic value of the samples resistivity would be arrived at. The Hall voltage was also determined more realistically by first applying the field in one direction and reversing the current direction, then reversing the field and reversing the current direction again. There was then a total of eight Hall voltages from which an average was used to arrive at a Hall coefficient.

From the average crystal voltage an effective sheet resistivity was determined using the following equation:

$$\rho_s = \frac{\pi}{\ell n2} \frac{\Delta V_c}{I_c} f \qquad (\Omega/\square) \qquad (5)$$

where ρ_s = sheet resistivity

ΔV_c = average crystal voltage

I_c = applied current

and f = dimensionless correction factor.

The Hall voltage was used to arrive at a Hall coefficient from the following equation:

$$R_s = 10^8 \left(\frac{\Delta V_s}{I_c B}\right) \qquad (cm^2/coul) \qquad (6)$$

where R_s = Hall coefficient

ΔV_s = Hall voltage

I_c = applied current

and B = applied magnetic field.

R_s was then used to calculate an effective sheet concentration, N_s, and mobility, μ_{eff}:

$$N_s = (qR_s)^{-1} \qquad (cm^{-2}) \qquad (7)$$

where q = electron charge

$$\mu_{eff} = \frac{R_s}{\rho_s} \qquad (cm^2/V\text{-sec}) \qquad (8)$$

The above equations are just averages depending upon the distribution in depth of the carrier concentration and the implantation factors. However, an electrical profile can show what fraction of the implanted atoms become substitutional, as well as the spatial location of the active atoms with respect to LSS theory (see Appendix F). The electrical profile was obtained by removing thin layers of the sample at a controlled rate. As each layer was removed, sheet resistivity and Hall coefficient measurements were taken and the number of carriers and their mobility was determined from the following equations (Ref 11):

$$\frac{(R_s)i}{(\rho_s)_i^2} - \frac{(R_s)i+1}{((\rho_s)_i+1)^2} = en_i \mu_i^2 d_i \ . \qquad (9)$$

and

$$\frac{1}{(\rho_s)_i} - \frac{1}{(\rho_s)_i+1} = en_i \mu_i d_i \qquad (10)$$

From equation (9) and (10) if follows that

$$\mu_i = \frac{(R_s/\rho_s^2)i}{(1/\rho_s)_i} \qquad (11)$$

and

$$n_i = \frac{(1/\rho_s)_i}{ed_i\mu_i}$$

(12)

where d_i is the thickness of the ith layer removed. The carrier concentration, $N_s(cm^{-2})$, is obtained from $n_i d_i$.

The degree of electrical compensation is defined as the ratio of donor to acceptor concentrations, $K = N_d/N_a$. It was not necessary to compute the values of N_d and N_a to find the compensation level. The only value that had to be determined was the concentration of total ionized impurities, P_I. This was done by using the well known Brooks-Herring relationship (Ref 11).

$$\mu_I = \frac{3h^3k^2p}{16^2e^3m^{*2}P_I} \frac{1}{\ell n(1+\oint) - \oint/(1+\oint)}$$

(13)

where $\oint = \frac{1}{2}(\frac{h}{e})^2(\frac{k}{m^*})(\frac{3p}{8})\frac{1}{3}$

h = Plank's constant

k = dielectric constant

e = electron charge

p = carrier concentration

P_I = concentration of total ionized impurities

m^* = effective hole mass

To be able to use the above equation, the mobility due to the ionized impurities (μ_I) must be known. This can be determined from the following equation:

$$\frac{1}{\mu} = \frac{1}{\mu_I} + \frac{1}{\mu_L}$$

(14)

assuming a value of 450 cm^2/V-sec (p-type samples) for lattice mobility (μ_L).

In order to calculate the compensation, K, the following two equations are used:

$$P_I = N_d + N_a \qquad (15)$$

$$p = N_d - N_a . \qquad (16)$$

These equations can be manipulated to give the following:

$$P_I - p = 2N_d \qquad (17)$$

$$P_I + p = 2N_a , \qquad (18)$$

from which follows:

$$K = \frac{P_I - p}{P_I + p} \qquad (19)$$

Using equations (13), (14) and (19) a series of curves can be formed by choosing a vaule for K, such that $0 \leq K \leq 1$, and a value for p, see Fig. 5.

The removal of these layers was obtained by etching the sample with a solution of H_2SO_4: 30% H_2O_2: H_2O in a ratio of 1:1:50, kept at 0°C. The etch removed thin layers of the sample at a predicted rate of 250 Å/min as determined by a Sloan Dektak microtopography on un-implanted sample. The contacts were protected at the same time to prevent degradation of the ohmic characteristics. This was done by covering the electrodes with black wax which has been mixed with trichlorethylene to a paint-like consistency. After profiling, the black wax was removed by washing the sample with trichlorethylene, thus revealing the contacts. Then the sample was taken to the Dektak to verify whether the etch was still etching at the determined rate. It was found that the etch actually proceeded at a slower than predicted

rate of 144 Å/min. After discovering this phenomena each sample was measured on the Dektak after profiling. The results showed that the etch rate was the same for the different implants and dosage. Therefore the implantation of the ions into the substrate must cause some change in the crystal for it to react in such a manner.

III. Experimental Results

Isochronal Annealing

This section deals mainly with temperature dependent parameters, obtained from surface measurements. The three different types of implants (GaAs:C^+, GaAs:Ga^+, C^+, GaAs: As^+, C^+) discussed individually and compared with each other to see if there was any verification of the predicted results. In addition an encapsulation study is included due to the problems which have been plaguing the process. This additional study helped to distinguish the effects of implantation versus the effects of encapsulation. The only data that was obtained was that of resistivity. No carrier concentration or mobility data was obtainable due to the Hall voltage being buried in the noise.

For the carrier concentration and mobility versus dose graphs, for all three implants, the numbered points 6, 7, 8, and 9 stand for 600°C, 700°C, 800°C, and 900°C, temperatures at which the samples were annealed.

GaAs:C^+

Annealing at the temperatures stated produced electrical activity in samples having a dose of $10^{13}C^+/cm^2$ and $10^{14}C^+/cm^2$ as shown in Fig. 6. For these two doses, it can be seen that the effective sheet resistivity is in the same order of magnitude for all annealing temperatures (T_A). The sample implanted with a dose of $10^{12}C^+/cm^2$ shows a very high resistivity, the same as that of the sample which was just encapsulated and annealed. It decreases sharply as does the encapsulated sample at 700°C and 800°C. For the temperature range of 800-900°C, the
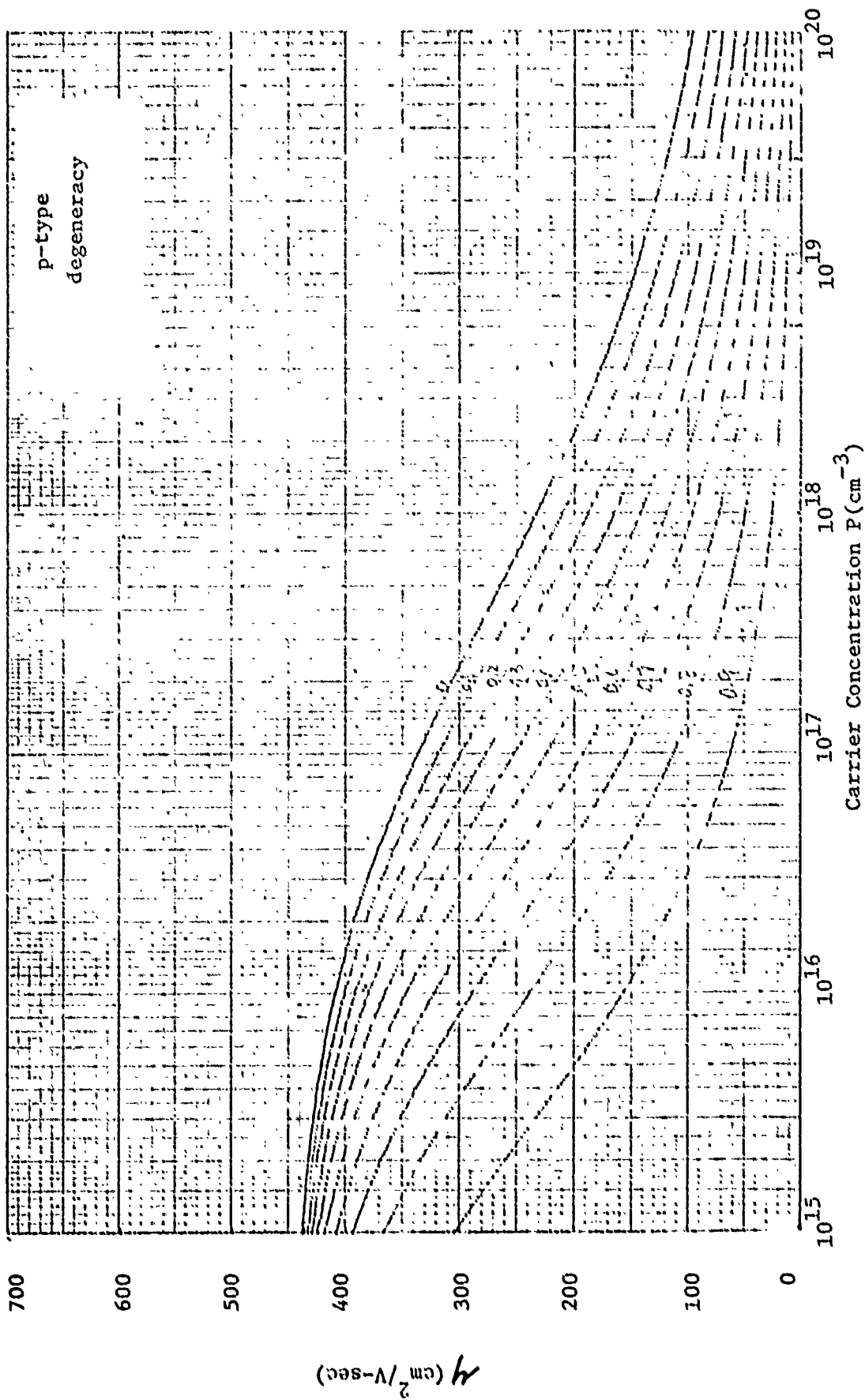
18

Fig. 5. Electrical compensation curves for p-type material
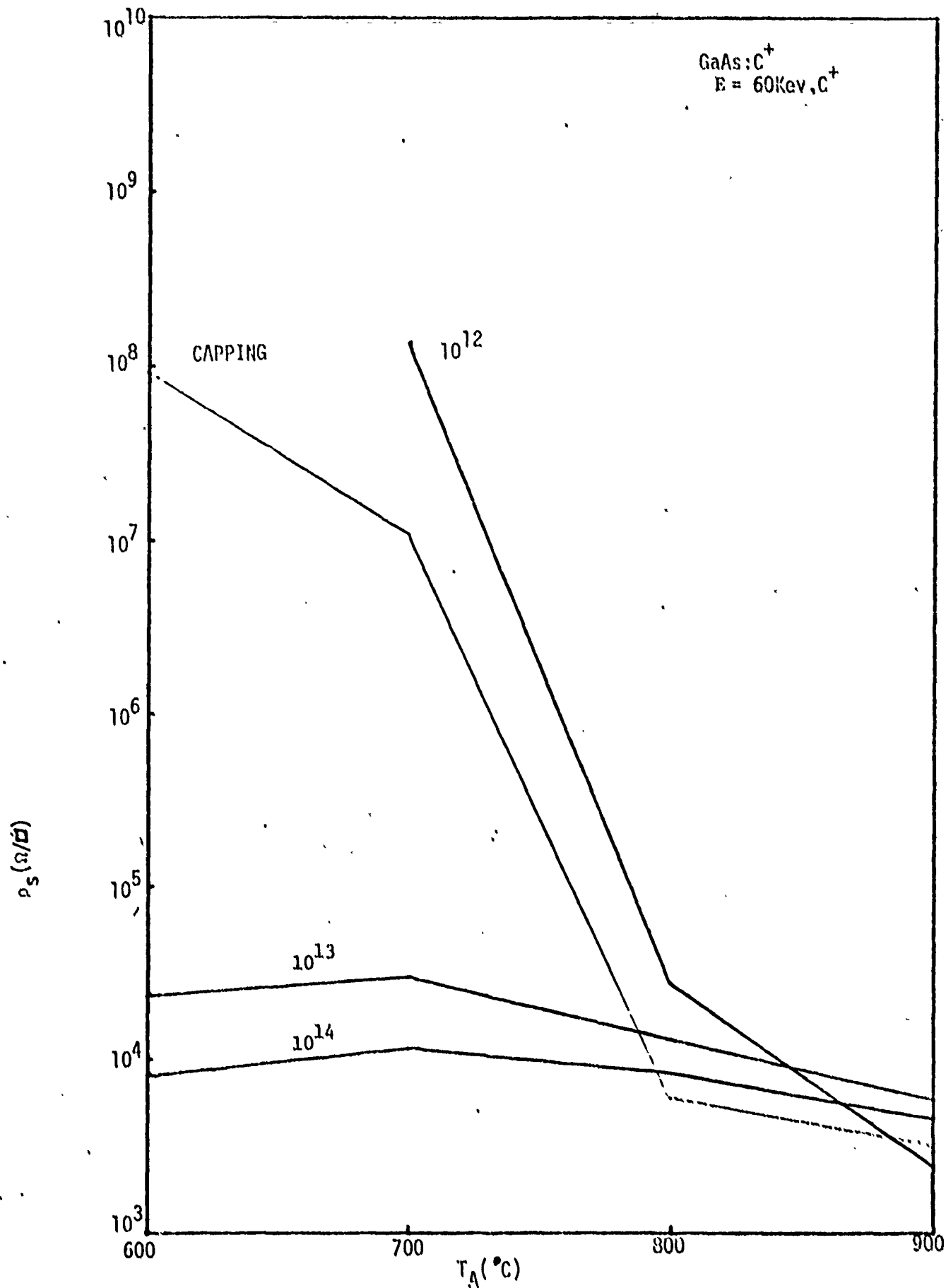
Fig. 6. Effective sheet resistivity
(ρ_s) vs. annealing temp. (T_A) for C^+
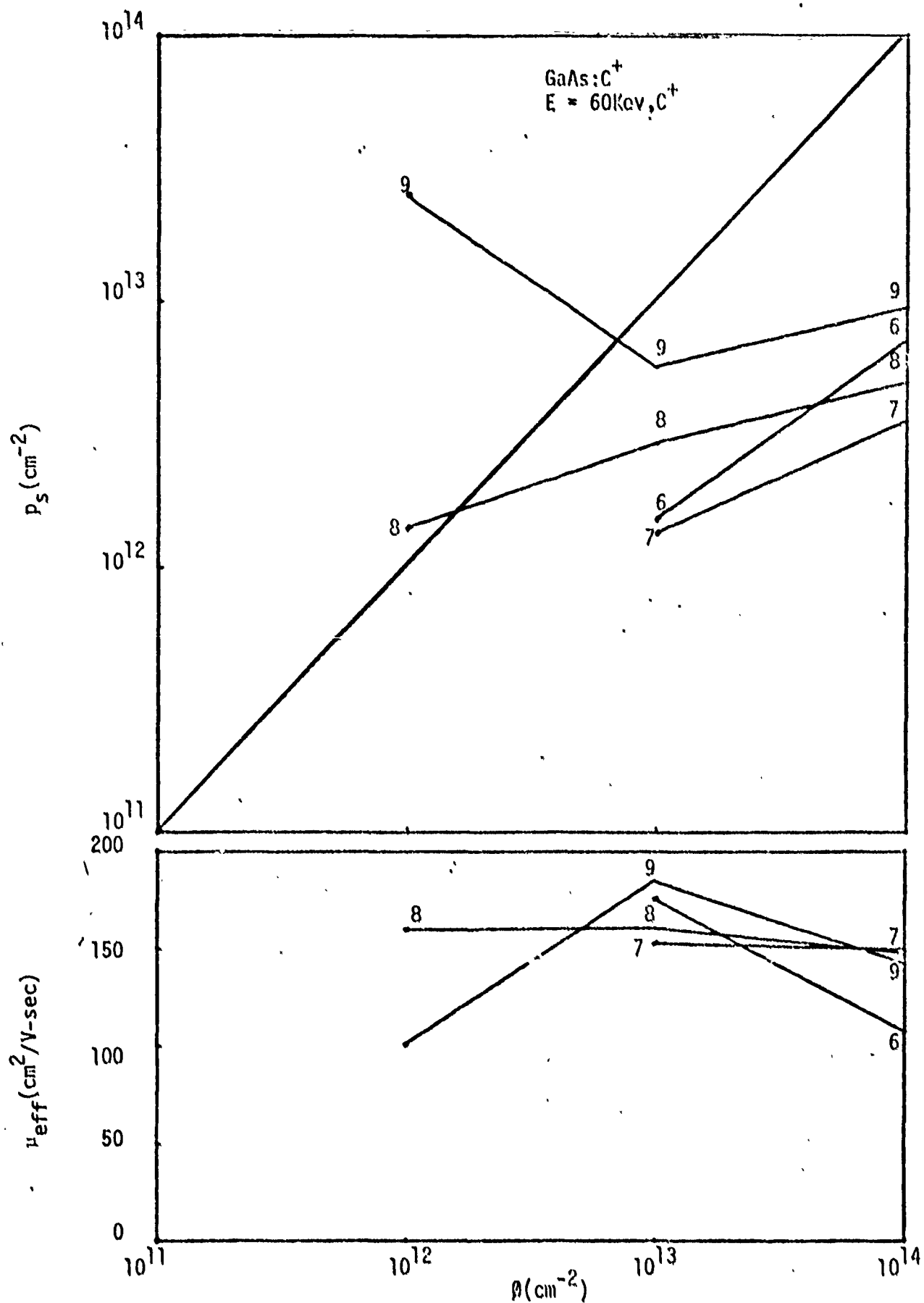
Fig. 7. Dependence of sheet hole concentration (p_s) and effective mobility upon C^+ dose ($\emptyset$)

resistivity is within the same order of magnitude for the different dosages and encapsulation. It can be said that there is some observed implantation effect in the $10^{13}C^+/cm^2$ and $10^{14}C^+/cm^2$ dosages at 600°C and 700°C samples. It is difficult to say this for the 800°C and 900°C range due to the gathering of all the curves at these temperatures.

Fig. 7 shows the annealing characteristics of effective sheet carrier concentration (P_s) and effective Hall mobility (μeff) for different temperatures. For $10^{12}C^+/cm^2$, carrier concentration and mobility were only obtainable for 800°C and 900°C. The carrier concentration for 800°C and 900°C increases with temperature but was higher than the implanted dosage. Also observed was the effect that the concentration decreased between 600°C and 700°C, and then increased between 700°C and 900°C for both the $10^{13}C^+/cm^2$ and $10^{14}C^+/cm^2$ samples. Although this trend was observed the concentration for $10^{14}C^+/cm^2$ at all annealing temperatures is higher than $10^{13}C^+/cm^2$ samples.

The doping efficiencies ($n = P_s/\emptyset$) were also determined in this study from the diagonal line drawn across the graphs. The results were compared with previous work done in this area by Sansbury, Harris and Shin (see Table I). For a dose of $10^{13}C^+/cm^2$, 900°C annealed, an efficiency of 57% was obtained while an efficiency of 9.5% was seen for a dose of $10^{14}C^+/cm^2$ annealed at 900°C. These values agree very well with Shin's findings even though an implantation energy of 60Kev was used. The low values obtained in previous studies were probably due to the low annealing temperatures and encapsulation methods used. In this study the same annealing temperatures and encapsulation procedures were used as by Shin (Ref 4).

Table I

Electrical Characteristics for Various Carbon ion Implantation (Ref 4)

$\emptyset (cm^{-2})$	E(Kev)	T(°C)	$\mu_{eff}(cm^2/V\text{-}sec)$	n(%)	Capping	Refferences
10^{13}	70	700	29	1.9	SiO_2	Sansbury
10^{14}	70	700	242	0.95	SiO_2	Sansbury
10^{15}	70	700	282	0.064	SiO_2	Sansbury
2×10^{14}	200	800	240	1.5	SiO_2	Harris
2×10^{14}	200	800	180	7.0[1]	SiO_2	Harris
10^{13}	120	900	218	50.0	Si_3N_4	Shin
10^{14}	120	900	224	12.0	Si_3N_4	Shin
10^{13}	60	900	185	57.0	Si_3N_4	This work
10^{14}	60	900	143	9.5	Si_3N_4	This work
10^{13}	120(Ga^+) 60(C^+)	800	125	87.0	Si_3N_4	This work
10^{14}	120(Ga^+) 60(C^+)	900	116	32.0	Si_3N_4	This work

[1]Sample implanted at 77°K

From the Hall mobility we can also see the effect that a dose of $10^{13} C^+/cm^2$ annealed at 900°C is more effective than a dose of $10^{14} C^+/cm^2$. The mobility is higher for $10^{13} C^+/cm^2$ dose than $10^{14} C^+/cm^2$ dose for all temperatures but lower than obtained in previous studies. This higher mobility could result from the encapsulation problem.

GaAs:Ga$^+$,C$^+$

The effective sheet resistivity (ρ_s) for GaAs: Ga$^+$,C$^+$ at the different annealing temperatures (Fig. 8) looks very much like what was observed for GaAs:C$^+$. The encapsulation and $10^{12} Ga^+$, C^+/cm^2 samples were high, while $10^{13} Ga^+$, C^+/cm^2 and $10^{14} Ga^+$, C+/cm^2 dose samples were in the 10^4 and 10^5 ohms per square ($\Omega/\square$) range. Another observation made was that all the dosages in the 800°C to 900°C range had lower resistivities than the GaAs:C$^+$ samples in the same range.

More observations can be made by looking at Fig. 9 which shows the effective sheet hole concentration and effective Hall mobility as a function of implanted dose ($\emptyset$). First, it is evident that for every temperature the hole concentration is greater for $10^{14} Ga^+$, C^+/cm^2 than $10^{13} Ga^+$, C^+/cm^2. The most promising fact is that at 900°C for $10^{14} Ga^+$, C^+/cm^2 the hole concentration is 3.23 x $10^{13}/cm^3$ which is an efficiency of 32%, a noticable improvement over just carbon implants. However for the $10^{13} Ga^+$, C^+/cm^2 dose at 800°C we have an efficiency of 87%, which is also a large increase over the same dose and temperature for just carbon implants.

The effective Hall mobility also showed a trend, in that at the $10^{14} Ga^+$, C^+/cm^2 dose the carbon implants alone were much higher than

Fig. 8. Evvective sheet resistivity (ρ_s)
vs. annealing temp. (T_A) for Ga$^+$, C$^+$
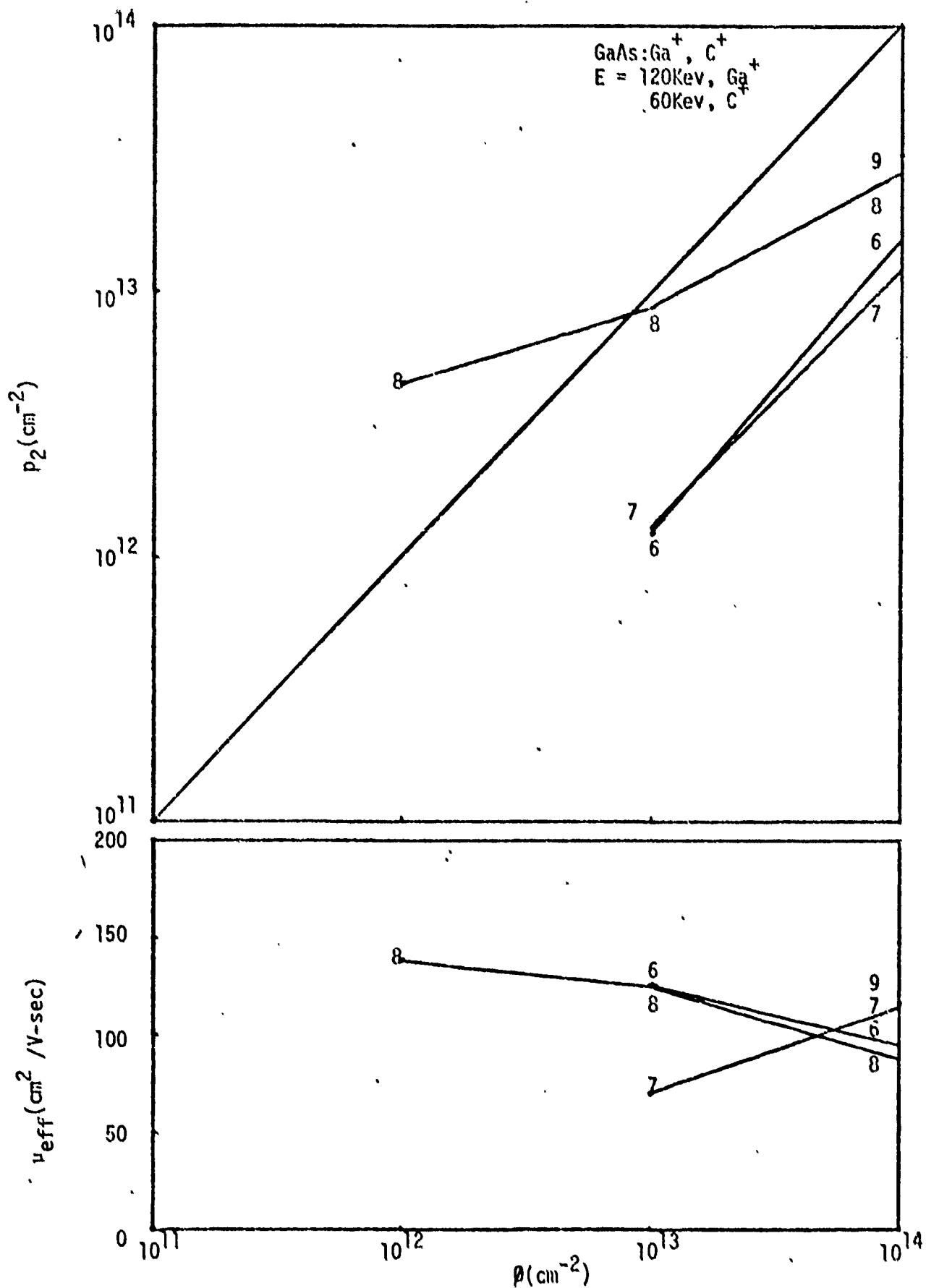
Fig. 9. Dependence of sheet hole concentration
(p_s) and effective mobility upon Ga^+, C^+ dose (ϕ)

the Ga^+, C^+ implants. In addition, there was an observed decrease in mobility from 10^{13} to 10^{14} doses in both cases for all temperatures except at 700°C.

GaAs:As^+, C^+

The effect sheet resistivity Fig. 10 shows the same trend as that of the C^+ and Ga^+, C^+ implants. Only a small difference can be seen in the 10^{14} dose where the sample has a little higher resistivity in the 600°C to 700°C temperature range. The graph also shows the same trend as the others, that is, from 800°C to 900°C they all come together. This makes it very hard to determine if this effect resulted from en-capsulation or implantation effect.

Looking at Fig. 11 we still observe the strange phenomena of the concentration being larger than the implanted dose this time for a $10^{13}As^+$, C^+/cm^2 dose at 900°C annealed. This characteristic may also have been observed for Ga^+, C^+ implants if it were possible to measure the Hall voltage. Also observed was that for 600°C and 700°C annealing temperatures at $10^{13}As^+$, C^+/cm^2 and $10^{14}As^+$, C^+/cm^2 dosages the con-centration was lower than for all the other implanted samples. Also, the efficiency for the sample annealed at 900°C at a dose of $10^{14}As^+$, C^+/cm^2 was 25%, which is lower than the Ga^+, C^+ implants but much higher than the C^+ implant.

The effective Hall mobility plot shows that at 10^{14} dose for all temperatures the mobility is in the same region as for C^+ implants but higher than for the Ga^+, C^+ implants. At the same time, the 10^{13} dose of As^+, C^+ implants for all temperatures had mobilities which were lower than the C+ implants and in the same region as the Ga^+, C^+ implants.
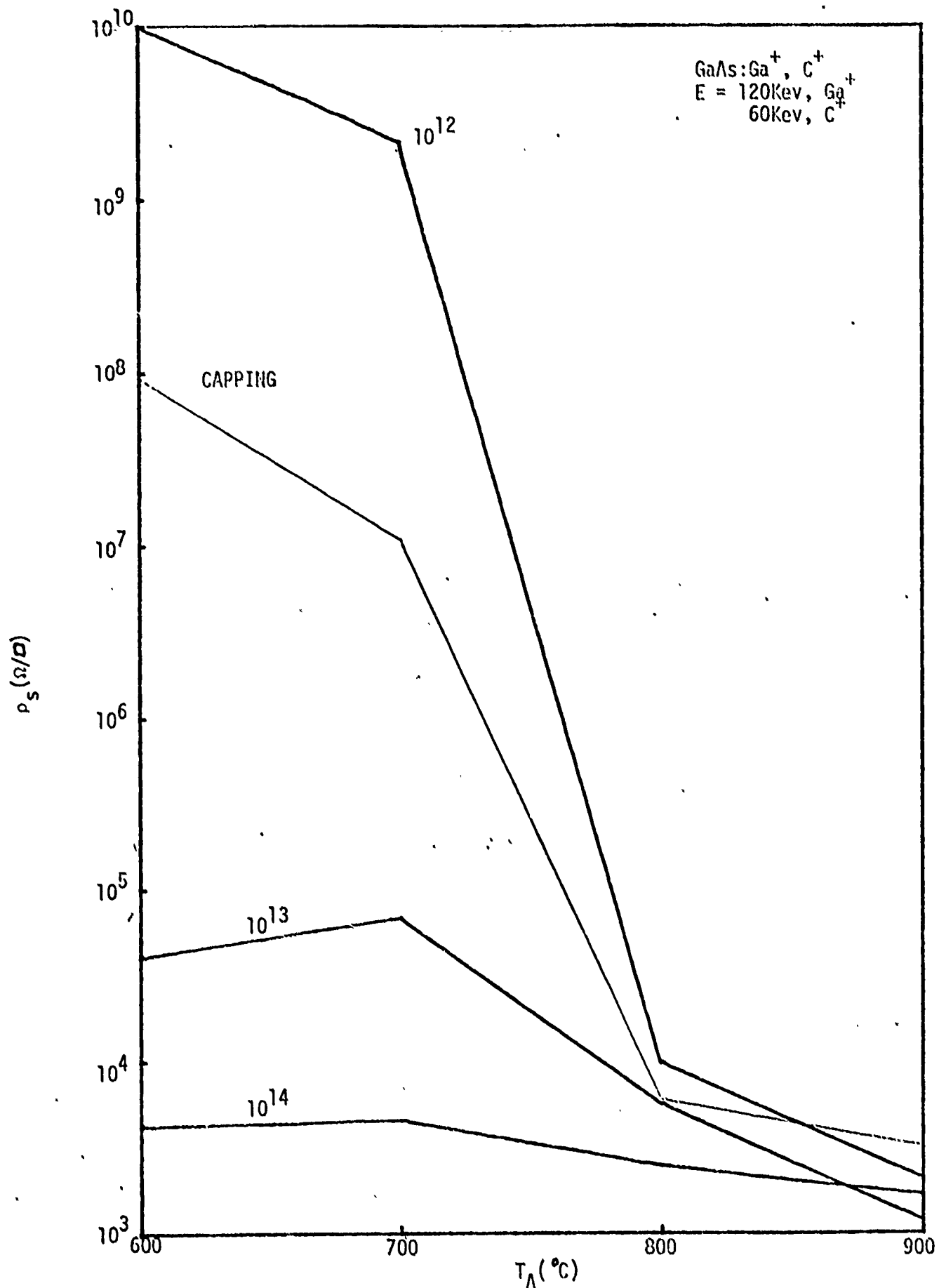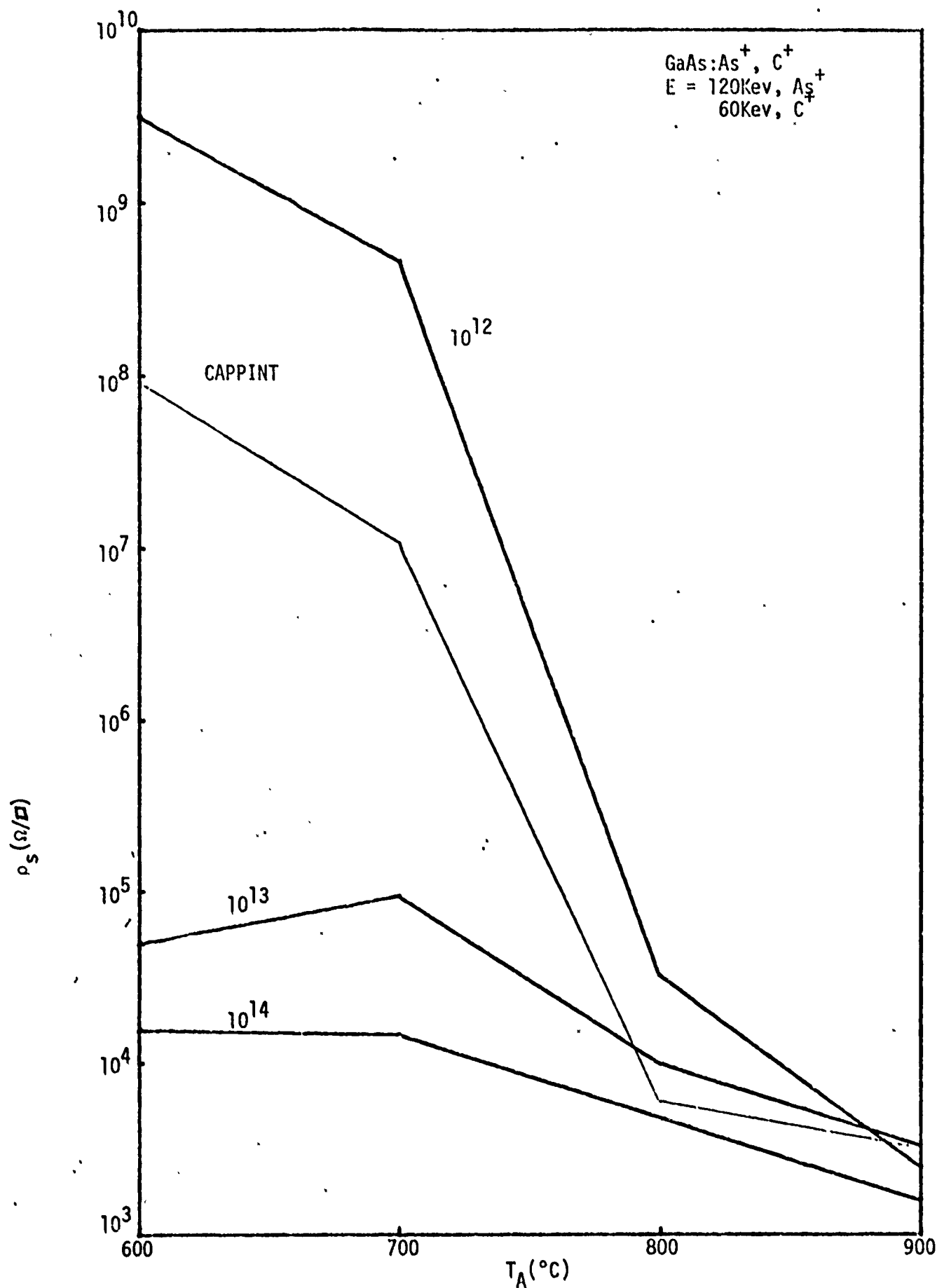
Fig. 10. Effective sheet resistivity (ρ_s)
vs. annealing temp. (T_A) for As$^+$, C$^+$
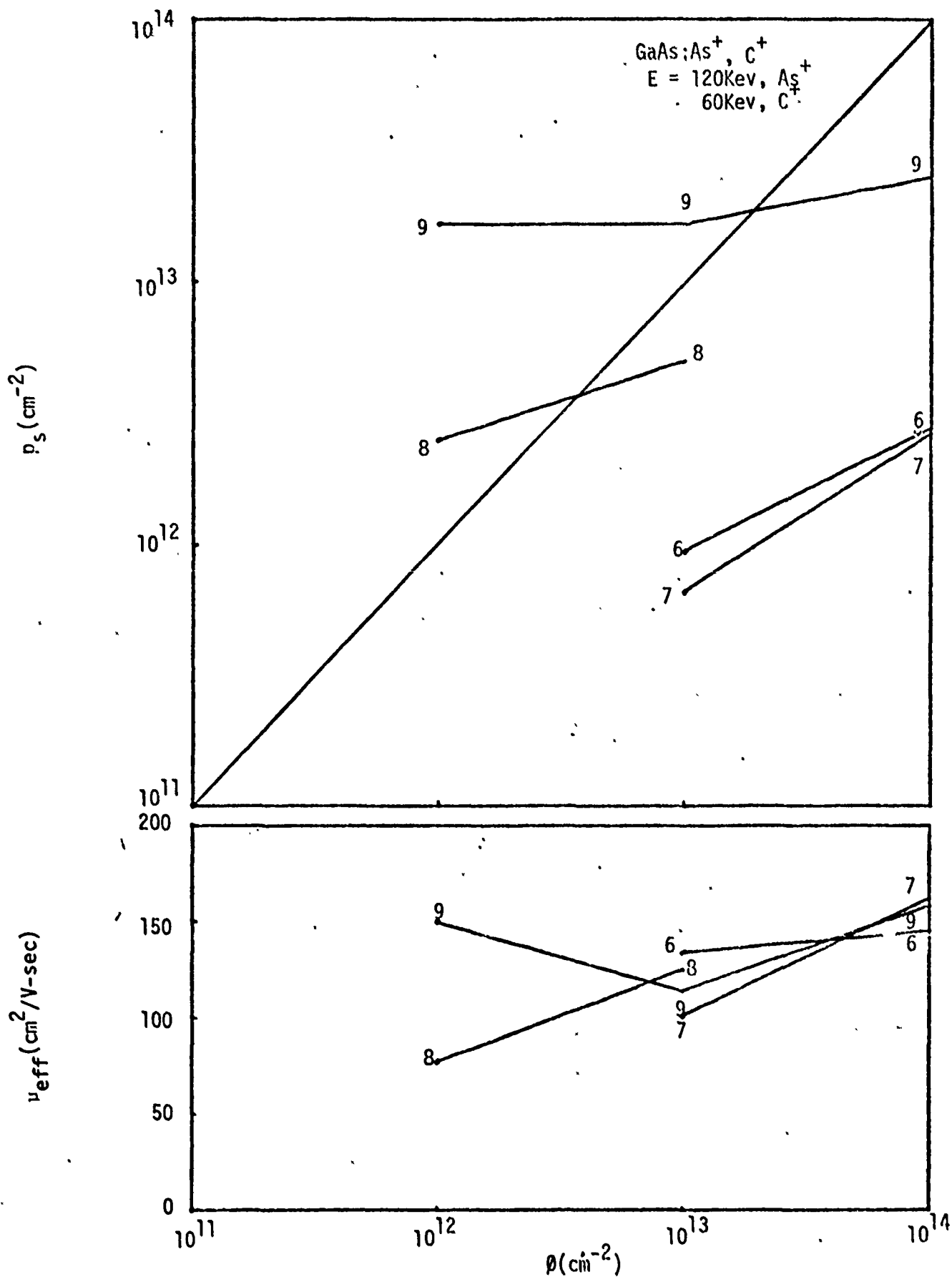
Fig. 11. Dependence of sheet hole concentration (p_s) and effective mobility upon As[+], C[+] dose ($\emptyset$)

GaAs:Ar$^+$

Due to problems in resolving whether or not the different trends in the data were due to implantation, damage or encapsulation argon implants were done. These implants would help in determing whether or not we were seeing implantation or damage effects, there was no experiment which could have been performed to separate the effects of encapsulation or implantation. The samples were prepared in the same matter as the C$^+$, Ga$^+$, As$^+$ samples, so the encapsulation effect would also be present. Only 600°C and 900°C annealed samples with 10^{12}, 10^{13} and 10^{14} doses of argon were made and encapsulated with 1000Å of Si_3N_4. Surface measurements were taken and resistivity, mobility and concentration were calculated, the results follow.

Table II

GaAs:Ar$^+$

T_A(°C)	ϕ(cm^{-2})	ρ_s(Ω/□)	μ (cm^2/V-sec)	P_s(cm^{-3})
600°C	10^{12}	5.8×10^7		
	10^{13}	2.8×10^7		
	10^{14}	5.2×10^6		
900°C	10^{12}	7163	154	5.7×10^{12}
	10^{13}	11000	120	4.7×10^{12}
	10^{14}	23600	91.5	3.0×10^{12}

We can see from the 600°C annealed samples that the resistivity stays fairly constant for the different dosages. While for the 900°C annealed samples the resistivity increased as the dose increased which can be taken as an increase in damage to the crystal. This damage effect can also be seen in the mobility and carrier concentration data.

Electrical Profiles

This section of the results will deal mainly with the electrical profiles of GaAs:As$^+$, C$^+$ ($\emptyset = 10^{12}$, $T_A = 900°C$), GaAs:As$^+$, C$^+$ ($\emptyset = 10^{13}$, $T_A = 900°C$), GaAs:As$^+$, C$^+$ ($\emptyset = 10^{14}$, $T_A = 900°C$), and GaAs:Ga$^+$, C$^+$ ($\emptyset = 10^{14}$, $T_A = 900°C$) which LSS profiles of As$^+$ and Ga$^+$ at 120Kev and C$^+$ at 60Kev. Two other profiles are also plotted on the same graph for each, those of V_{GA} and V_{AS} vacancies due to the experimental work of Chiang and Pearson (Ref 10). Also each plot, beneath the profile, has Brooks-Herring mobility compared to the mobility determined experimentally. Using the above information and bulk hole concentration, the electrical compensation coefficient, K, could be determined from the curves (see Figure 5).

When first comparing all the profiles, it is surprising to observe the similarities between them. The value of hole concentration is a maximum near the surface of about 10^{18} and $10^{19} cm^{-3}$, and slowly varies with depth, x. The most interesting one is the GaAs:As$^+$, C$^+$ ($\emptyset = 10^{12}$, $T_A = 900°C$), sample where it is observed that the experimentally determined profile is actually higher than the LSS profiles which might be anticipated from the effective sheet carrier concentration measurement. The reason for this phenomena is not very definite but after looking at the Hall voltages it was observed that most of the readings were less than 100 microvolts, voltages at which error is probable.

Out of all the samples, the most interesting to compare are GaAs:As$^+$, C$^+$ (Fig. 14) and GaAs:Ga$^+$, C$^+$ (Fig. 15). The maximum concentration of GaAs:As$^+$, C$^+$ almost reaches $10^{19} cm^{-3}$ near the surface, which is the highest compared to the rest. GaAs:Ga$^+$, C$^+$ follows the

LSS profile better than GaAs:As$^+$, C$^+$, which deviates from it near the tail and behaves as the gallium vacancies (V$_{GA}$) profile. The same result might have been observed in the GaAs:Ga$^+$, C$^+$ sample if it were etched a little further. Looking at the mobility curves we see that for GaAs:Ga$^+$, C$^+$ the mobility is more constant with depth where as for GaAs:As$^+$, C$^+$ the mobility varies quite a bit in the implant region, and starts to smooth out, as if it was due to the V$_{GA}$. While looking at the electrical compensation curves GaAs:Ga$^+$, C$^+$ shows a much better K near the surface and increasing with depth which is logical. The GaAs:As$^+$, C$^+$ sample shows a compensation curve which is virtually invarient with depth, neglecting the first two points which are due to very small Hall voltages.
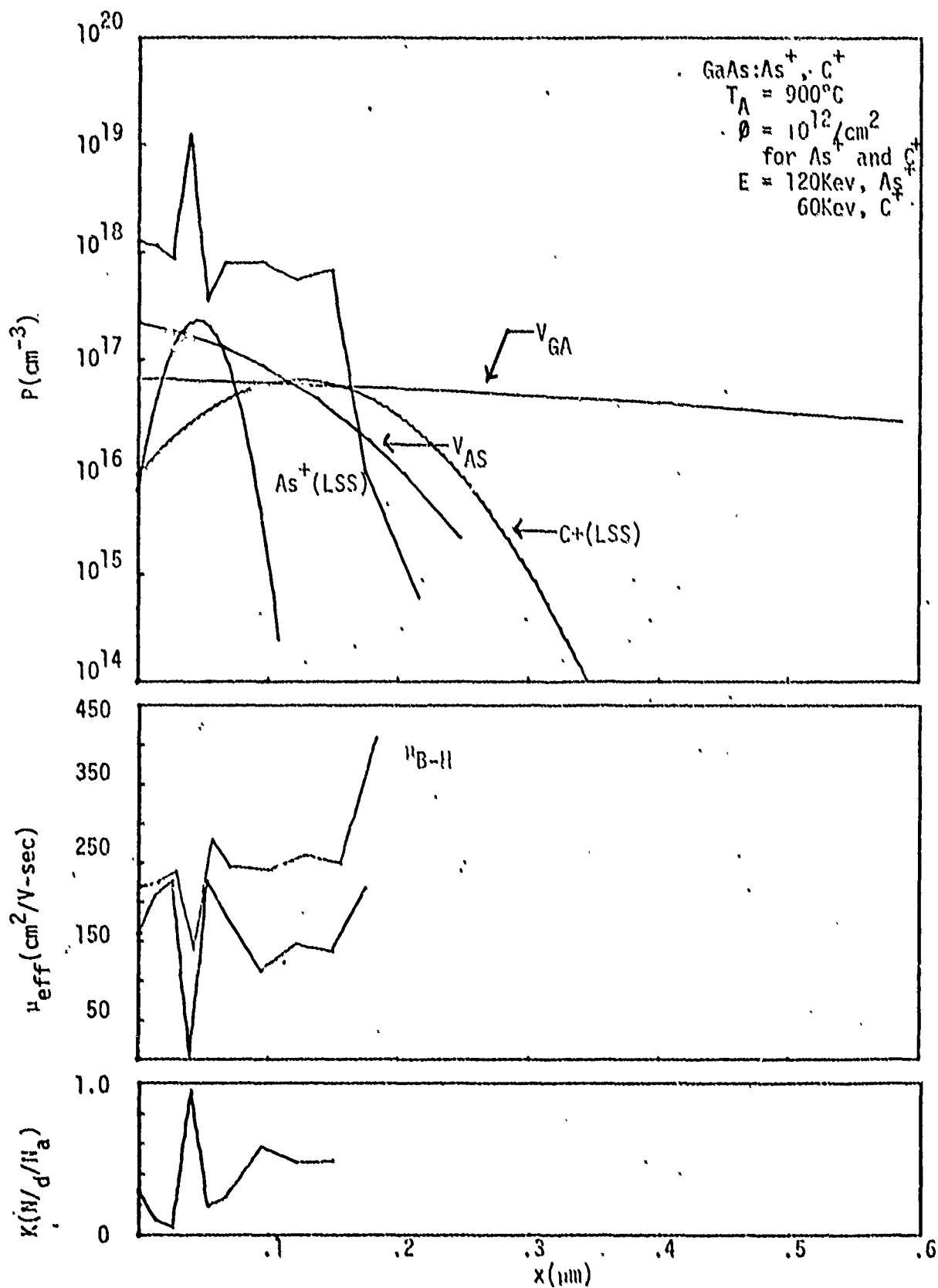
Fig. 12. Electrical profiles of carrier concentration (P), mobility (μ_{eff}) and electrical compensation factor (K) with depth (x)
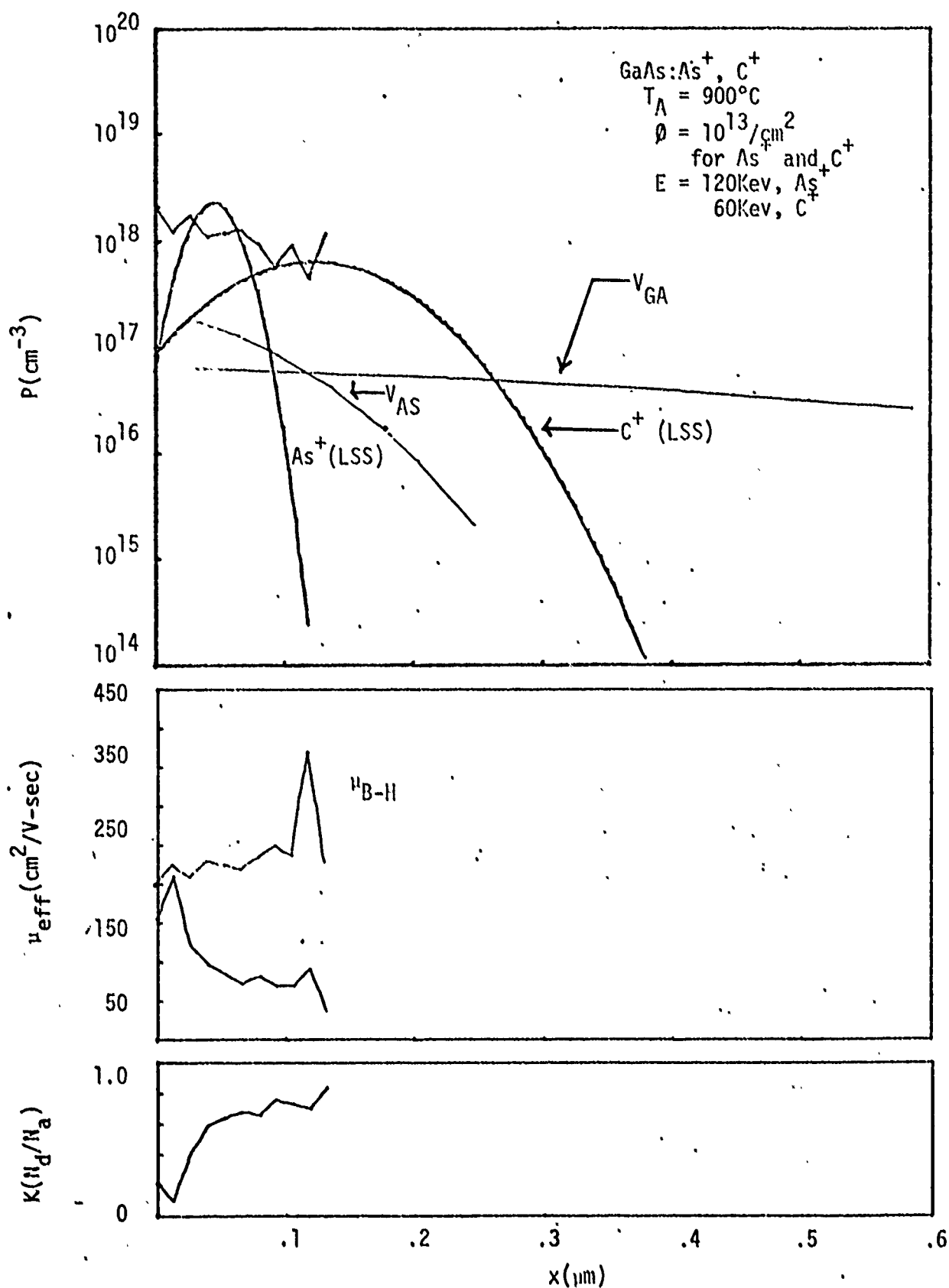
Fig. 13. Electrical profiles of carrier concentration (P), mobility (μ_{eff}) and electrical compensation factor (K) with depth (x)

34

Fig. 14. Electrical profiles of carrier concentration (P), mobility (μ_{eff}) and electrical compensation factor (K) with depth (x)

10^{20}

10^{19}

10^{18}

10^{17}

$P(cm^{-3})$

10^{16}

10^{15}

GaAs:Ga$^+$, C$^+$
T_A = 900°C
ϕ = 10^{14}/cm^2 for
Ga$^+$ and C$^+$
E = 120Kev, Ga$^+$
60Kev, C$^+$

V_{GA}

Ga$^+$
(LSS)

V_{AS}

C$^+$(LSS)

450

350

250

150

50

$\mu_{eff}(cm^2/V\text{-}sec)$

^{11}B-H

1.0

$K(N_d/N_a)$

0

.1   .2   .3   .4   .5   .6

x(µm)
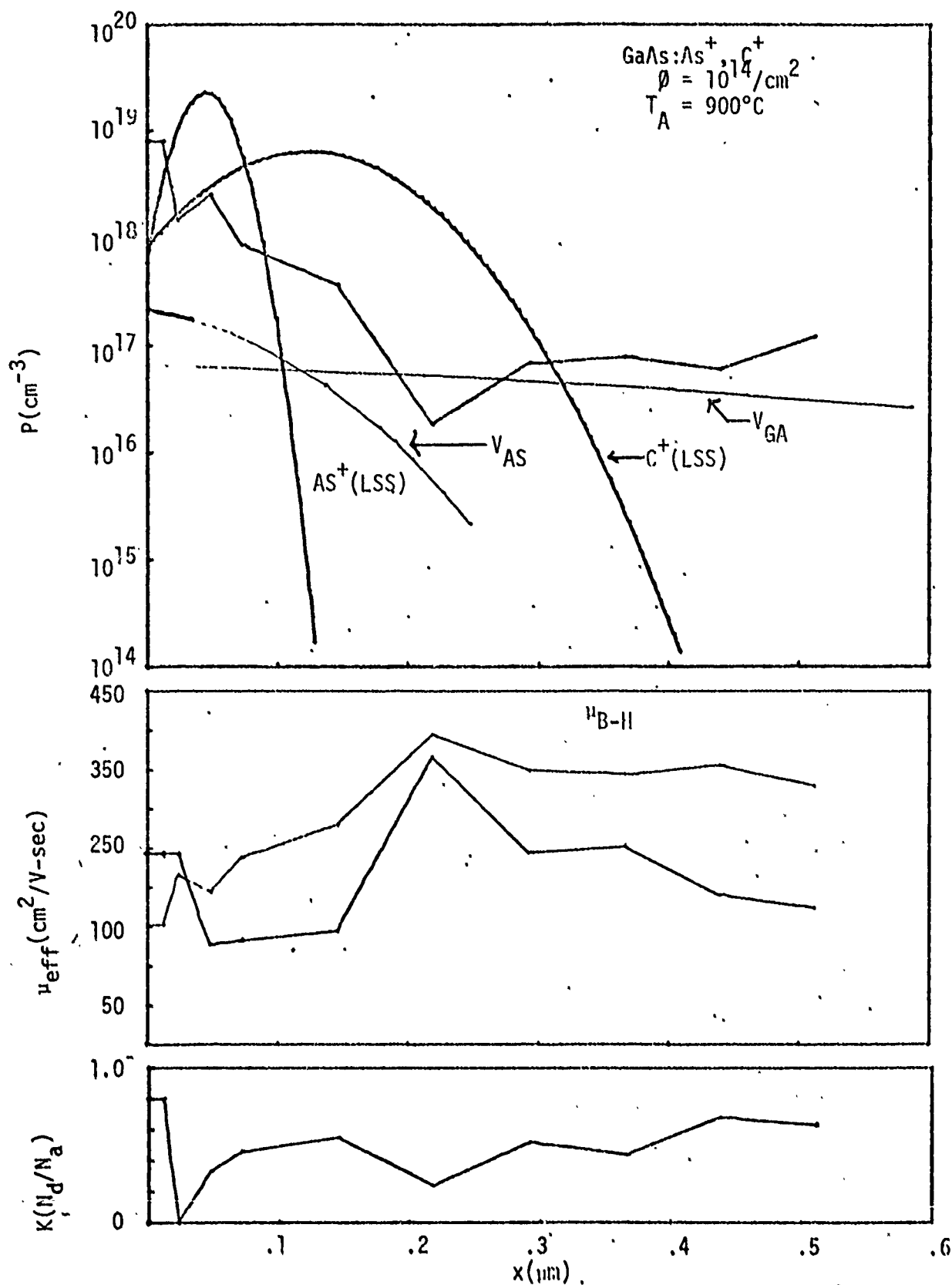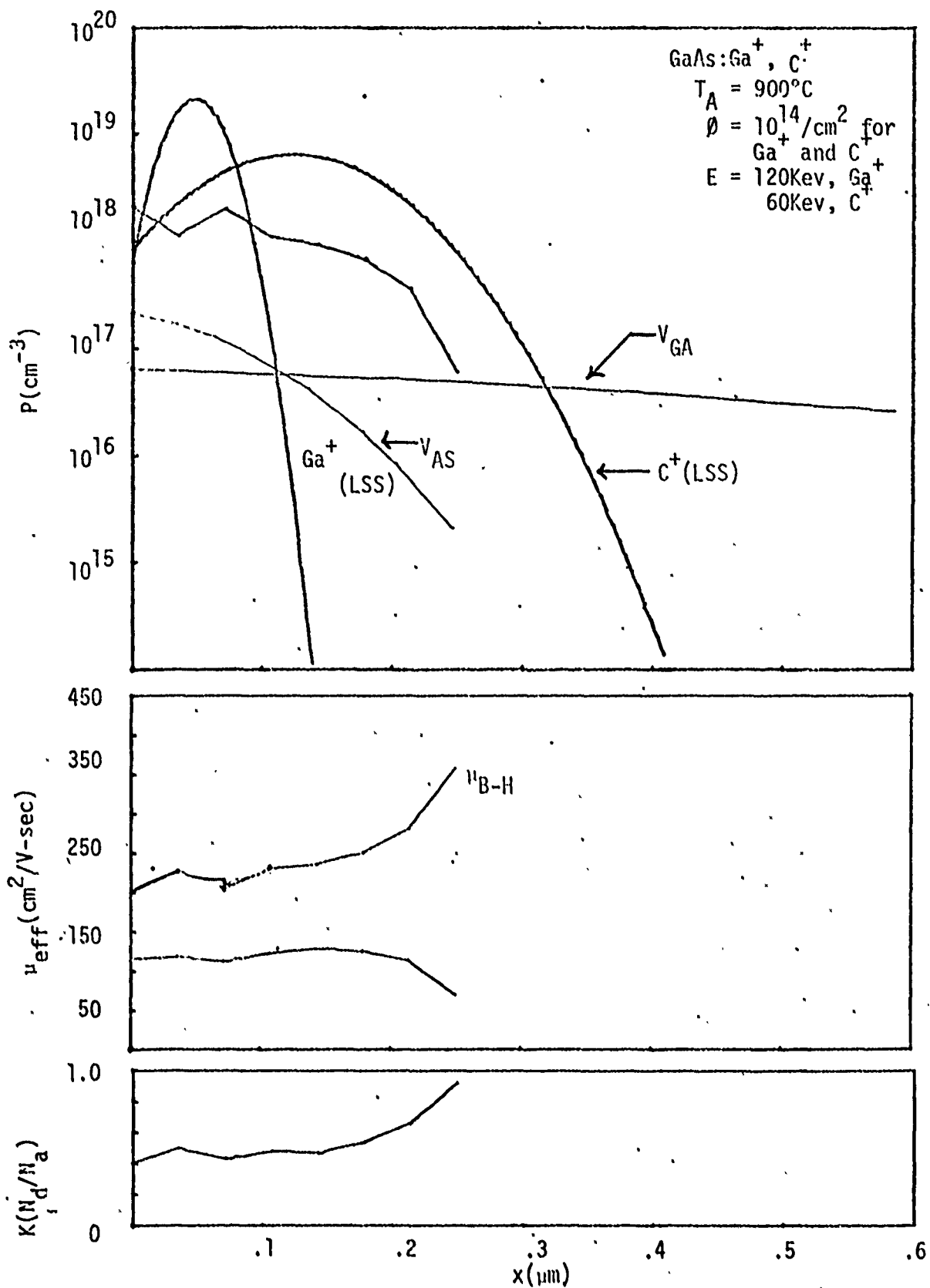
Fig. 15. Electrical profiles of carrier concentration (P), mobility (μ_{eff}) and electrical compensation factor (K) with depth (x)

IV. Discussion of Experimental Results

From the data acquired on isochronal annealing two features can be seen immediately. For all the different types of implants, at annealing temperatures of 600°C and 700°C, the resistivities for the 10^{12} samples are very high, higher than just encapsulated samples (no implants). As data from GaAs:Ar$^+$ implants indicated that the resistivity is high. However, 10^{13} and 10^{14} dose samples for all implants show low resistivity. Such a difference in resistivity with dosage suggest there is a strong dose dependence with annealing temperature. In fact, it is so dose dependent that no matter what the implants may be, this effect was observed. At the higher annealing temperatures the resistivities are all the same order of magnitude, suggesting that the thermal effect predominates the resistivity. At these temperatures the encapsulation (with which there has been some problem) could act as a sink, drawing out the Ga and As, and causing vacancies to be formed. This possibility may also account for the observations made with the 10^{12} dose samples, annealed at 800°C and 900°C which show a doping efficiency of greater than 100%. The Hall voltages measured on these samples were less than 100 microvolts and very unstable which is subject to error. The crystal voltage (which was higher and more in the range of accuracy of the equipment) also displayed a strange phenomena. Crystal voltages from one configuration to the next changed drastically, sometimes by a factor of six, indicating there was severe inhomogeneity, as can be seen in Fig. 16 by checking for ohmic contacts in different configurations.
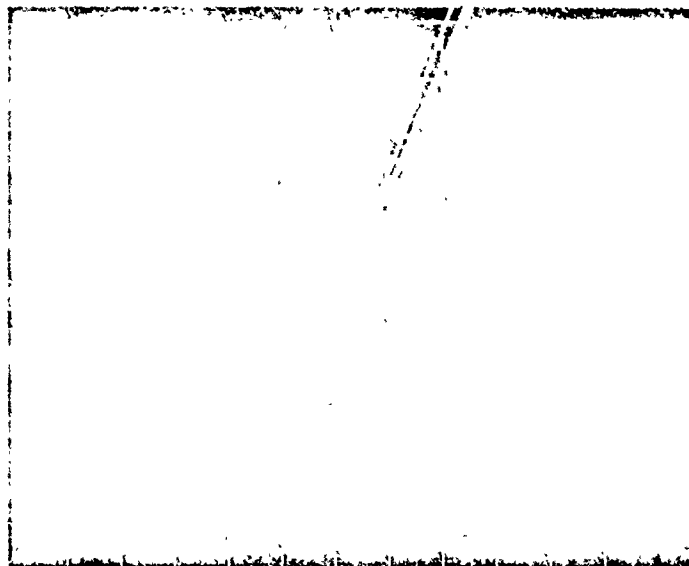
Fig. 16. I-V curves for different
sample configurations

The first intention of this study was to reproduce the results of C^+ implantation by Shin and to increase the efficiency of C^+ implants by co-implantation with Ga^+. The other objective was to look into the possibility of controlling the degree of compensation by co-implantation of As^+ and possibly forming n-type layers. The amphoteric nature of C^+ in GaAs allows co-implantation by forcing C^+ into arsenic or gallium sites. Perhaps the most convincing data obtained were for samples implanted with 10^{14} dose and annealed at 700°C as shown in Table III. In the table, the resistivity of samples implanted with C^+ is lower by two orders of magnitude. Co-implantation of Ga^+ enhances the doping efficiency while As^+ co-implantation reduces the electrical activity. The encapsulation used for the present study appears to be superior to SiO_2 layers used by Sansbury or Harris (Ref 8,9) as can be seen from the table.

Table III

Electrical Characteristics of 10^{14} dose and 700°C annealed samples

Sample	ρ_s (Ω/□)	μ_{eff} (cm^2/V-sec)	P_s (cm^{-2})
Encapsulation	1.08×10^7		
GaAs:Ar$^+$	5.01×10^6		
GaAs:C$^+$	1.17×10^4	150	3.57×10^{12}
GaAs:Ga$^+$, C$^+$	4.56×10^3	114	1.20×10^{13}
GaAs:As$^+$, C$^+$	1.47×10^4	162	2.63×10^{12}
Sansbury	2.72×10^4	242	9.50×10^{11}

In addition, other supporting results are shown in the 10^{14}/cm^2, 900°C annealed, GaAs:Ga$^+$, C$^+$, GaAs:As$^+$, C$^+$, and GaAs:C$^+$ samples. Efficiency is highest for the Ga$^+$ co-implantation with a value of 32%. As$^+$ gave an efficiency of 25% while C$^+$ alone was only 9.5%. Although the As$^+$, C$^+$ co-implantation was expected to be lower than the C$^+$ alone, the gross damage effect due to the heavy ions seems to aid the efficiency obtained in these samples at this annealing temperature. The annealing behavior discussed so far can be more clearly observed from the profiles obtained. The GaAs:As$^+$, C$^+$ sample of 10^{12}/cm^2 dose, annealed at 900°C (Fig. 12) is most peculiar of them all, since the concentration profile is substantially higher than either LSS profile or sublattice vacancy profile obtained from Pearson and Chiang (Ref 10). This phenomena suggest, as stated previously, the encapsulation may act as a sink and enhance the out-diffusion of the sublattice atoms. It would account for the high p-type concentration at the surface. This observation is reinforced by comparing the concentration profile to the

gallium vacancy profile, which changes as a complementary error function. The concentration profiles appear to be independent of dose or type of implants as can be seen by comparing Fig. 12 through 15. This indicates that it is very difficult to separate the effects due to encapsulation from those due to implantation using the profiles. In spite of this difficulty, it is still interesting to compare the $10^{14}/cm^2$, 900°C samples of GaAs:As$^+$, C$^+$ and GaAs:Ga$^+$, C$^+$. It can be observed from Fig. 14 and 15 that Ga$^+$ co-implantation gives better profile integrity. This can be seen from the low compensation coefficient near the Ga$^+$ implanted area. On the other hand the As$^+$ co-implantation gives a broad profile with no sharp average change in compensation with depth. The high bulk concentration ($10^{19}/cm^3$) near the surface in Fig. 14 might be due to damage enhanced doping effect as indicated by the high compensation value in this region.

V. Summary, Conclusion and Recommendations

This thesis looked at the possibility of co-implantation of As^+ and Ga^+ with C^+, in order to reduce the electrical activity of the dopant in one case, and to increase in the other. GaAs was doped with C^+ alone and with equal doses of As^+ and Ga^+ to maintain the stoichiometry of the crystal. The samples were all encapsulated with the same material and thickness, and annealed for the same period of time. The samples implanted with C^+ only were done to verify Shin's results and used as a reference for the co-implantation samples. Only surface measurements were made on most of the samples due to the extended amount of time required to profile each one. The only ones that were profiled were the 900°C annealed samples. Only five profiles are presented because it was not possible to obtain any Hall voltages on the others in addition, the etch rate was so fast that after two etches the implanted region was passed. The samples for which no profiles were obtained could have been run aga-n but the ion implantation facility was not operational, and therefore could not produce more samples. From the data obtained, it is seen that some of the predicted results were verified.

The results presented in this thesis have shown to some extent that the addition of Ga^+ or As^+ implants to the primary implants C^+, has an effect on the doping efficiency and crystal lattice. This effect is due to the encapsulation, which may be acting as a sink for out-diffusion of gallium vacancies, the enhancement of site location due to the Ga^+, As^+ implants, and possibly the damage of the sublattice. All these effects contribute to the efficiency which was observed, but they must be studied separately to see how much each one contributes.

41

Additional work should be carried out in co-implantation for controlling the stoichiometry of the GaAs, which shows some promise for ion implantated layers. More measurements should be acquired to show the reproducibility of this process. The encapsulation which has plagued this work should be more thoroughly researched as it hinders the observation of implantation results. The damages and reactions produced by the implantation of Ga^+ and As^+ should also be looked into. Temperature dependence measurements should be made to better distinguish the effects which are dominant in the conduction process. Different annealing schemes should also be tried. For example, annealing could be done after Ga^+ or As^+ implantation, followed by implantation of the primary species with post annealing. This may relieve some of the damage due to the heavy ion implantation.

Bibliography

1. Heckingbottom, R. and T. Ambridge. "Ion·Implantation in Compound Semiconductor-An Approach Based on Solid State Theory." Radiation Effects, 17:31-36 (1973).

2. Hilsum, C. Semiconducting III-V Compounds. New York: Pergamon Press, 1961.

3. Lyons Jr., R. P. Ion Implantation of Diatomic Sulfur into GaAs. Unpublished thesis. Wright-Patterson Air Force Base, Ohio: Air Force Institute of Technology, September 1974.

4. Shin, B. K. "Carbon Ion Implanted Gallium Arsenide." Applied Physics Letter, 29:438-440 (October 1976).

5. Stolte, C. A. "Dual Species Ion Implantation into GaAs." To be published.

6. Woodcock, J. M. "Enhancement of the Donor Activity of Implanted Selenium in GaAs by Gallium Implantation." Applied Physics Letter, 28:226-227 (February 1976).

7. Rodine, E. T., R. R. Berliner and B. K. Shin. Ion Implantation in Compound Semiconductors. AFAL-TR-76-218. Wright-Patterson Air Base, Ohio: Air Force Avionics Laboratory, January 1977.

8. Sansbury, J. D. Technical Report no. 4725-2 (prepared under ARPA Center for Materials Research Contract C-0218 and National Science Foundation Grant GK 4290), Stanford U., Stanford, Calif., 1970 (unpublished).

9. Harris, J. S. International Conference on Ion Implantation in Semiconductors. Edited by I. Ruge and J. Granl (Springer-Verlay, Berline, 1971, pg. 1571).

10. Chiang, S. Y. and G. L. Pearson. "Properties of Vacancy Defects in GaAs Single Crystals." Journal of Applied Physics, 46:2986-2991 (July 1975).

11. Johansson, N. G. E. and J. W. Mayer. "Technique Used in Hall Effect Analysis of Ion Implanted Si and Ge." Solid State Electronics, 13:317-335 (1970).

12. Gibbons, J. F., W. S. Johnson and S. W. Mylroie. Projected Range Statistics Semiconductors and Related Materials. Pennsylvania: Halsted Press.

13. Johnson, W. S. and J. F. Gibbons. Projected Range Statistics in Semiconductors. Stanford U. Bookstore.

14. Sze, S. M. Physics of Semiconductor Devices. New York: Wiley-Interscience, 1969.

Appendix A

Definition of Symbols

$F(g)$	a foreign atom in the gas phase
F_{GA}, F_{AS}	a foreign atom on a Ga or As lattice site in GaAs
F_{si}	a foreign atom on a Si lattice site
h	a hole in the valence band
e	an electron in the conduction band
x, 'and'	supperscripts denote neutral, single positively charged and single negative charged species respectively
V_{AS}, V_{GA}	a vacant site in the arsenic or gallium sublattice
Ga_i, As_i	a gallium or arsenic atom on an interstitial site

(Ref 1)

Appendix B

Flow rates for deposition of Si_3N_4

Film		Si_3N_4 (SCCM)	N_2 (SCCM)	NH_3 (SCCM)	N_2 (SCCM)	Set Temp	T.C. nv	Time	Hold Temp	Before AFTE	LN_2
Ga^+, C^+	Si_3N_4	80	500	200	500	725	29.7	30 sec	200°C	B/A	LN_2
	Si_3N_4	80	500	200	500	725	29.7	30 sec	200°C	B/A	LN_2
	Si_3N_4	80	500	200	500	725	29.7	30 sec	200°C	B/A	LN_2
As^+, C^+	Si_3N_4	80	500	200	500	725	29.8	30 sec	200°C	B/A	LN_2
	Si_3N_4	80	500	200	500	725	29.8	30 sec	200°C	B/A	LN_2
	Si_3N_4	80	500	200	500	725	29.8	30 sec	200°C	B/A	LN_2
C^+	Si_3N_4	80	500	200	500	725	29.8	30 sec	200°C	B/A	LN_2
	Si_3N_4	80	500	200	500	725	29.8	30 sec	200°C	B/A	LN_2
	Si_3N_4	80	500	200	500	725	29.8	30 sec	200°C	B/A	LN_2

Order	Color	SiO$_2$ Thickness Range* (μm)	Si$_3$N$_4$ Thickness Range (μm)
	Silicon	0-0.027	0-0.020
	Brown	0.027-0.053	0.020-0.040
	Golden Brown	0.053-0.073	0.040-0.055
	Red	0.073-0.097	0.055-0.073
	Deep Blue	0.097-0.010	0.073-0.077
1st	Blue	0.10-0.12	0.077-0.093
	Pale Blue	0.12-0.13	0.093-0.10
	Very Pale Blue	0.13-0.15	0.10-0.11
	Silicon	0.15-0.16	0.11-0.12
	Light Yellow	0.16-0.17	0.12-0.13
	Yellow	0.17-0.20	0.13-0.15
	Orange Red	0.20-0.24	0.15-0.18
1st	Red	0.24-0.25	0.18-0.19
	Dark Red	0.25-0.28	0.19-0.21
2nd	Blue	0.28-0.31	0.21-0.23
	Blue-Green	0.31-0.33	0.23-0.25
	Light Green	0.33-0.37	0.25-0.28
	Orange Yellow	0.37-0.40	0.28-0.30
2nd	Red	0.40-0.44	0.30-0.33

* The ratio of refractive index $\dfrac{n(Si_3N_4)}{n(SiO_2)} = \dfrac{1.97}{1.48} = 1.33 = \dfrac{SiO_2 \text{ thickness}}{Si_3N_4 \text{ thickness}}$

Fig. C.1 Color corresponding to varying thicknesses of the deposited layer

Appendix D

Table IV

GaAs:C$^+$

$\phi(cm^{-2})$	$T_A(°C)$	$\rho_s(\Omega/\square)$	$\mu_{eff}(cm^2/V\text{-sec})$	$P_s(cm^{-2})$
10^{12}	600			
	700	1.35×10^8		
	800	2.78×10^4	160	1.41×10^{12}
	900	2.47×10^3	101	2.50×10^{13}
10^{13}	600	2.34×10^4	176	1.52×10^{12}
	700	3.02×10^4	153	1.35×10^{12}
	800	1.32×10^4	161	2.94×10^{12}
	900	5.90×10^3	185	5.73×10^{12}
10^{14}	600	8.07×10^3	108	7.14×10^{12}
	700	1.17×10^4	150	3.57×10^{12}
	800	8.43×10^3	148	5.00×10^{12}
	900	4.58×10^3	143	9.50×10^{12}

Table V

GaAs:Ga$^+$, C$^+$

$\phi(cm^{-2})$	$T_A(°C)$	$\rho_s(\Omega/\square)$	$\mu_{eff}(cm^2/V\text{-sec})$	$P_s(cm^{-2})$
10^{12}	600	$\sim 10^{10}$		
	700	2.14×10^9		
	800	9.92×10^3	138	4.50×10^{12}
	900	2.10×10^3		
10^{13}	600	4.05×10^4	126	1.23×10^{12}
	700	6.84×10^4	70	1.30×10^{12}
	800	5.71×10^3	125	8.70×10^{12}
	900	1.20×10^3		
10^{14}	600	4.21×10^3	95	1.56×10^{13}
	700	4.56×10^3	114	1.20×10^{13}
	800	2.48×10^3	88	2.80×10^{13}
	900	1.67×10^3	116	3.32×10^{13}

Table VI

GaAs:As$^+$, C$^+$

$\phi(cm^{-2})$	$T_A(°C)$	$\rho_s(\Omega/\square)$	$\mu_{eff}(cm^2/V\text{-sec})$	$P_s(cm^{-2})$
10^{12}	600	3.10×10^9		
	700	4.60×10^8		
	800	3.26×10^4	77	2.50×10^{12}
	900	2.50×10^3	150	1.66×10^{13}
10^{13}	600	4.95×10^4	134	9.43×10^{11}
	700	9.41×10^4	101	6.58×10^{11}
	800	9.97×10^3	125	5.00×10^{12}
	900	3.31×10^3	114	1.66×10^{13}
10^{14}	600	1.55×10^4	145	2.77×10^{12}
	700	1.47×10^4	162	2.63×10^{12}
	800			
	900	1.59×10^3	158	2.50×10^{13}

Table VII

Encapsulation

$T_A(°C)$	$\rho_s(\Omega/\square)$
600	9.22×10^7
700	1.08×10^7
800	6.02×10^3
900	3.20×10^3

$$n_{mas}(R_p) = \frac{\emptyset}{\Delta R_p \sqrt{2\pi}} \qquad\qquad (B.2)$$

Using these equations and range tables, the theoretical profiles can be determined. For this thesis range tables could not be found for the implantation of As^+ and Ga^+ into GaAs, but a computer program which was available at AFAL, produced the tables required.

The distribution can be tailored for the required needs by coating the surface with some substance which has a stopping power close to that of the substrate. Therefore the peak is moved closer to the surface by a distance equal to the coating. Then you would have a higher concentration at the surface and one junction instead of two (see Fig. B.1).
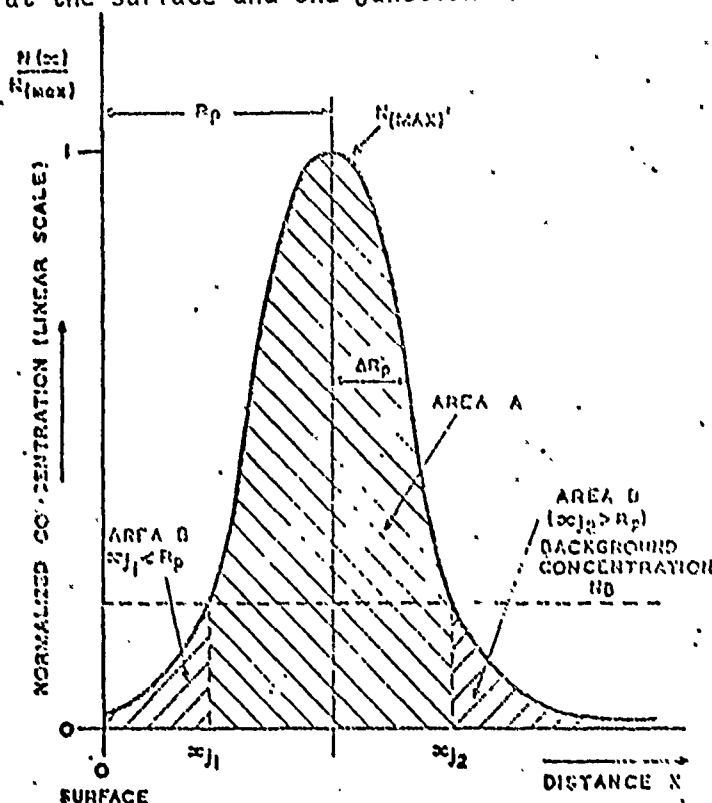

Fig. 5.5. A typical theoretical Gaussian ion distribution with depth. R_p is the projected range, ΔR_p the standard deviation and N_0 the background doping concentration. x_{j_1} and x_{j_2} are the positions of p-n junctions if type conversion is produced. (See text for explanation of areas A and B.)

Fig. B.1 Theoretical Gaussian implant profile (Ref 13)

LSS RANGE STATISTICS FOR ARSENIC

ION GALLIUM ARSENIDE

SUBSTRATE PARAMETERS-

	GALLIUM	ARSENIDE
Z	31	33
M	69.723	74.923
N	.221-E+23	.221-E+23
RHO/R	.725-E+01	.7+13E+01
EPS/E	.341E-02	.3293E-02
C/SE	.19-6E+02	.20-3E+02
γ0	.931	1.000
G-γ/E	.9397	1.0000
S/C	.145E+04	

ION-ARSENIC

Z	33
M	74.920

ELECTRONIC CROSS SECTIONS OF
LINDHARD,SCHARFF,SCHIOTT

ENERGY (KEV)	PROJECTED RANGE (MICRONS)	PROJECTED STANDARD DEVIATION (MICRONS)	STANDARD	
25				
30				
40				
50				
60				
70				
80				
90				
100				
110				
120				
130				
140				
150				
160				
170				
180				
190				
200				
225				
250				
275				
300				
325				
350				
375				
400				
425				
450				
475				
500				
550				
600				
650				
700				
750				
800				
850				
900				
1000				

LSS RANGE STATISTICS FOR GALLIUM

IN GALLIUM ARSENIDE

			PROJECTED RANGE	PROJECTED STANDARD DEVIATION	RANGE	STANDARD DEVIATION	NUCLEAR
ENERGY			(MICRONS)	(MICRONS)	(MICRONS)	(MICRONS)	dE/dx
(KEV)							

SUBSTRATE PARAMETERS -

	GALLIUM	ARSENIDE
Z	31	33
M	69.721	74.320
N	.2214E+23	.2214E+23
RHO/R	.7734E+01	.7564E+01
EPS/E	.3511E-02	.3665E-02
C/SE	.1975E+02	.2037E+02
MU	1.390	1.075
GAMMA	1.0000	.9937
SRC	.1335E+04	

ION — GALLIUM

Z	31
M	69.720

ELECTRONIC CROSS SECTIONS OF
LINDHARD, SCHARFF, SCHIOTT

Appendix F

Range-Profiles of Ion Implanted Samples

The Linhard, Scharff and Schiott (LSS) theory was developed on the bases that the implant ions were accelerated into a amorphous target. The reason for this line of thought is that the theory for range distribution in crystals is not well developed (Ref 12). To overcome this problem the crystal is oriented off axis when being implanted or ordered from the manufacture grown in a specific direction. Therefore, the implanted ions will not channel and the substrate will look more amorphous in nature. The GaAs substrates used in this thesis were implanted 7° off the axis of the [100] direction. The range distribution will depend on the energy, mass and nuclear charge of the ion, as well as the mass and density of the substrate. The combination of these parameters results in a Gaussian distribution which has some range and standard deviation (Fig. B.1).

The impurity density from the surface can be represented by the following equation:

$$n(\lambda) = \frac{\emptyset}{\Delta R_p \sqrt{2\pi}} \exp\left[\frac{-(x - R_p)^2}{2 \Delta R_p^2}\right] \qquad (B.1)$$

where x = depth from surface,

$\emptyset$ = ion dose/cm^2,

ΔR_p = standard deviation in projected range,

and R_p = projected range.

The peak impurity concentration can be determined by setting x equal to R_p:

$$n_{mas} (R_p) = \frac{\emptyset}{\Delta R_p \sqrt{2\pi}} \qquad (B.2)$$

Using these equations and range tables, the theoretical profiles can be determined. For this thesis range tables could not be found for the implantation of As^+ and Ga^+ into GaAs, but a computer program which was available at AFAL, produced the tables required.

The distribution can be tailored for the required needs by coating the surface with some substance which has a stopping power close to that of the substrate. Therefore the peak is moved closer to the surface by a distance equal to the coating. Then you would have a higher concentration at the surface and one junction instead of two (see Fig. B.1).
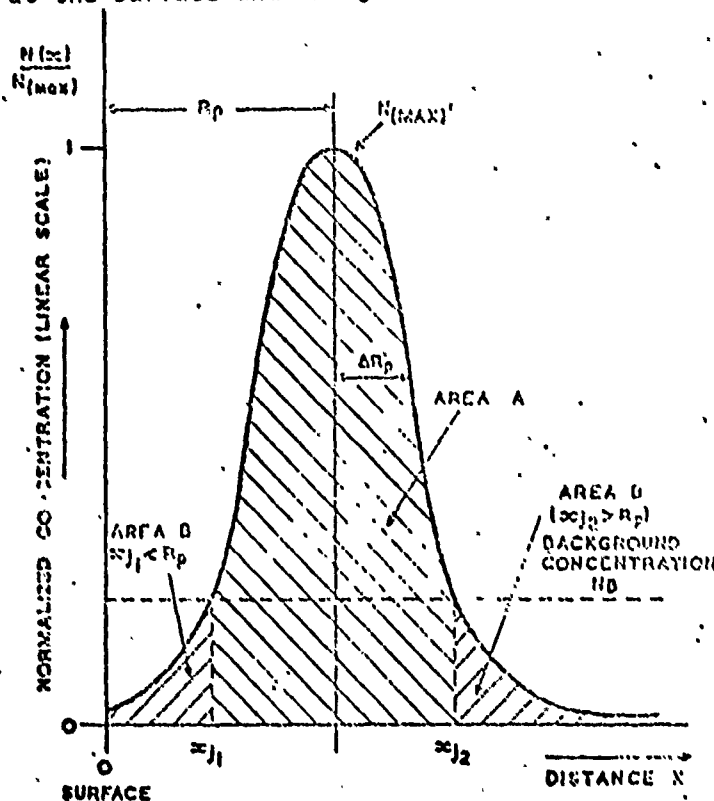

Fig. 5.5. A typical theoretical Gaussian ion distribution with depth. R_p is the projected range, ΔR_p the standard deviation and N_0 the background doping concentration. X_{j_1} and X_{j_2} are the positions of p-n junctions if type conversion is produced. (See text for explanation of areas A and B.)

Fig. B.1 Theoretical Gaussian implant profile (Ref 13)

VITA

Michael Stefiniw was born August 23, 1954 in Passaic, New Jersey.
He graduated from Morris Catholic High School in 1972 and attended
Stevens Institute of Technology in Hoboken, New Jersey. He received
his commission from ROTC in May 1976. His first assignment was the
Air Force Institute of Technology, Wright Patterson Air Force Base,
Ohio, where he is enrolled in the Graduate Electro-Optics program.

<div align="right">

Permanent Address: Smithtown Road
Hackettstown,
New Jersey 07840

</div>

REPORT DOCUMENTATION PAGE		READ INSTRUCTIONS BEFORE COMPLETING FORM
1. REPORT NUMBER GEO/PH/77-4	2. GOVT ACCESSION NO.	3. RECIPIENT'S CATALOG NUMBER
4. TITLE (and Subtitle) DIFFERENTIAL-HALL IMPURITY PROFILING OF GaAs, CO-IMPLANTED WITH Ga+, C+ AND As+, C+		5. TYPE OF REPORT & PERIOD COVERED MS Thesis
		6. PERFORMING ORG. REPORT NUMBER
7. AUTHOR(s)		8. CONTRACT OR GRANT NUMBER(s)
9. PERFORMING ORGANIZATION NAME AND ADDRESS Air Force Institute of Technology (AFIT/EN) Wright-Patterson AFB, Ohio 45433		10. PROGRAM ELEMENT, PROJECT, TASK AREA & WORK UNIT NUMBERS
11. CONTROLLING OFFICE NAME AND ADDRESS AFAL/DHE Air Force Avionics Laboratory Wright-Patterson AFB, Ohio 45433		12. REPORT DATE October, 1977
		13. NUMBER OF PAGES 54
14. MONITORING AGENCY NAME & ADDRESS(if different from Controlling Office)		15. SECURITY CLASS. (of this report) Unclassified
		15a. DECLASSIFICATION/DOWNGRADING SCHEDULE

16. DISTRIBUTION STATEMENT (of this Report)

Approved for public release; distribution unlimited.

17. DISTRIBUTION STATEMENT (of the abstract entered in Block 20, if different from Report)

Approved for public release; IAW AFR 190-17

JERRAL F. GUESS, Captain, USAF
Director of Information

18. SUPPLEMENTARY NOTES

19. KEY WORDS (Continue on reverse side if necessary and identify by block number)
Ion Implantation
III-V Compounds
GaAs
Co-Implantation

20. ABSTRACT (Continue on reverse side if necessary and identify by block number)
Co-implantation of Ga+ or As+ with C+ has produced p-type conduction in GaAs substrate. Sheet resistivity and Hall effect measurements were made and differential Hall effect measurements were carried out using a guarded van der Pauw system. These measurements were carried out on 10^{12}, 10^{13}, and 10^{14} dosage samples annealed at 600, 700, 800, and 900°C for fifteen minutes. Doping efficiency of 87% was obtained in the 800°C annealed sample implanted with 10^{13} ins/cm² of Ga+ and C+ which is much higher than for the C+ alone implants. Samples annealed at 900°C, 10^{14} ins/cm² of Ga+ and C+ had an efficiency of

32.3% which is also higher than the C^+ alone implants. Carbon implants alone had a 57% efficiency when annealed at 900°C with a dose of $10^{13}/cm^2$ and 9.5% when annealed at 900°C with a dose of $10^{14}/cm^2$, which verifies previous work done with carbon implants.